NUREG/CR-1023
ORNL/NUREG/TM-351

ornl

OAK
RIDGE
NATIONAL
LABORATORY

UNION
CARBIDE

Multirod Burst Test Program Progress Report for April-June 1979

R. H. Chapman

Prepared for the U.S. Nuclear Regulatory Commission
Office of Nuclear Regulatory Research
Under Interagency Agreements DOE 40-551-75 and 40-552-75

OPERATED BY
UNION CARBIDE CORPORATION
FOR THE UNITED STATES
DEPARTMENT OF ENERGY

Printed in the United States of America. Available from
National Technical Information Service
U.S. Department of Commerce
5285 Port Royal Road, Springfield, Virginia 22161

NUREG/CR-1023
ORNL/NUREG/TM-351
Dist. Category R3

Contract No. W-7405-eng-26

Engineering Technology Division

MULTIROD BURST TEST PROGRAM PROGRESS REPORT FOR APRIL–JUNE 1979

R. H. Chapman

Manuscript Completed – October 23, 1979
Date Published – November 1979

Prepared for the
U.S. Nuclear Regulatory Commission
Office of Nuclear Regulatory Research
Washington, D.C. 20555
Under Interagency Agreements DOE 40-551-75 and 40-552-75

NRC FIN No. B0120

Prepared by the
OAK RIDGE NATIONAL LABORATORY
Oak Ridge, Tennessee 37830
operated by
UNION CARBIDE CORPORATION
for the
DEPARTMENT OF ENERGY

CONTENTS

FOREWORD

This report summarizes progress and preliminary results of the Multirod Burst Test (MRBT) Program [sponsored by the Division of Reactor Safety Research of the Nuclear Regulatory Commission (NRC)] for the period April–June 1979.

Work on this program was reported initially in Volume I of a four-volume series entitled *Quarterly Progress Report on Reactor Safety Programs Sponsored by the NRC Division of Reactor Safety Research*. Prior reports of MRBT activities in this series are:

Report No.	Pages	Period covered
ORNL/TM-4729	70–72	July–September 1974
ORNL/TM-4805	102–110	October–December 1974
ORNL/TM-4914	78–104	January–March 1975
ORNL/TM-5021	76–98	April–June 1975

Beginning with the period July–September 1975, work on this program is documented in reports titled *Multirod Burst Test Program Progress Report*. Prior reports in this series are:

Report No.	Period covered
ORNL/TM-5154	July–September 1975
ORNL/NUREG/TM-10	October–December 1975
ORNL/NUREG/TM-36	January–March 1976
ORNL/NUREG/TM-74	April–June 1976
ORNL/NUREG/TM-77	July–September 1976
ORNL/NUREG/TM-95	October–December 1976
ORNL/NUREG/TM-108	January–March 1977
ORNL/NUREG/TM-135	April–June 1977

In mid-1978, a duplicate report identification system was instituted whereby an NRC report number is also assigned to NRC-sponsored work. Previous progress reports issued in this category include:

NUREG report No.	ORNL report No.	Period covered
NUREG/CR-0103	ORNL/NUREG/TM-200	July–December 1977
NUREG/CR-0225	ORNL/NUREG/TM-217	January–March 1978
NUREG/CR-0398	ORNL/NUREG/TM-243	April–June 1978
NUREG/CR-0655	ORNL/NUREG/TM-297	July–December 1978
NUREG/CR-0817	ORNL/NUREG/TM-323	January–March 1979

Topical reports pertaining to research and development carried out by this program are:

1. R. H. Chapman, compiler, *Characterization of Zircaloy-4 Tubing Procured for Fuel Cladding Research Programs*, ORNL/NUREG/TM-29 (July 1976).
2. W. E. Baucum and R. E. Dial, *An Apparatus for Spot Welding Sheathed Thermocouples to the Inside of Small-Diameter Tubes at Precise Locations*, ORNL/NUREG/TM-33 (August 1976).
3. W. A. Simpson, Jr., et al., *Infrared Inspection and Characterization of Fuel-Pin Simulators*, ORNL/NUREG/TM-55 (November 1976).
4. R. H. Chapman et al., *Effect of Creep Time and Heating Rate on Deformation of Zircaloy-4 Tubes Tested in Steam with Internal Heaters*, NUREG/CR-0343 (ORNL/NUREG/TM-245) (October 1978).

The following limited-distribution quick-look and data reports have been issued by this program:

1. R. H. Chapman, compiler, *Quick-look Report on MRBT No. 1 4 × 4 Bundle Burst Test*, Internal Report ORNL/MRBT-2 (September 1977).
2. R. H. Chapman, compiler, *Quick-look Report on MRBT No. 2 4 × 4 Bundle Burst Test*, Internal Report ORNL/MRBT-3 (November 1977).
3. R. H. Chapman, *Quick-look Report on MRBT No. 3 4 × 4 Bundle Burst Test*, Internal Report ORNL/MRBT-4 (August 1978).
4. R. H. Chapman et al., *Bundle B-1 Test Data*, ORNL/NUREG/TM-322 (June 1979).
5. R. H. Chapman et al., *Bundle B-2 Test Data*, ORNL/NUREG/TM-337 (August 1979).

SUMMARY

The majority of our single-rod burst tests have been conducted with a cladding heating rate of about 28°C/sec. Also, all of the single-rod tests conducted prior to this reporting period were surrounded by an unheated shroud which remained at about 340°C throughout the test transient. The burst temperature data from the 28°C/sec transient heating tests were correlated with the burst pressure by an empirically fitted equation. A limited number of burst tests were conducted (and reported earlier) to scope the effect of lower heating rates. The results of the tests indicated that the correlation should have a heating rate effect included.

This was shown to be the case by appropriate data selected from the literature. In particular, isothermal creep rupture (100 sec hold time) and very slow (0.3°C/sec) transient heating data were used. The previous correlation was modified to include a normalized (to 28°C/sec) heating-rate factor and shown to represent our 28°C/sec transient data and the selected literature data quite well. In an exercise to see whether it would predict the results of intermediate-heating-rate tests, the modified correlation predicted the results of our low-heating-rate test series with surprisingly good accuracy. Further optimization of the correlation, based on extensive published data over a range of test conditions, is planned in order to broaden the base of applicability.

Posttest examination of the B-3 test was essentially completed during this reporting period. Enlarged (about 5×) photographs of the bundle cross sections were analyzed to obtain strains in each tube at each cross section. The strain matrix thus produced was then used to construct deformation profiles of the tubes and the loss in coolant-channel flow area as a function of axial position.

The data confirmed previously reported observations that the burst strains in the B-3 bundle were greater than those observed in the B-1 and B-2 tests. This, presumably, is the result of the lower heating rate and lower test temperature for the B-3 test (9.5°C/sec heating rate and about 760°C test temperature for B-3, compared with 30°C/sec heating rate and 865°C test temperature for B-1 and B-2). Since the deformation of the B-3

bundle was greater, there was also a greater loss in coolant-channel flow area.

A number of equipment demonstration tests were conducted to check out and verify proper operation of the recently procured shroud power supply and its associated control components. This equipment is portable and can be used in conjunction with either the multirod or single-rod test facility. Demonstration tests were conducted in both facilities, and these showed that the average shroud temperature can be controlled to follow the average test specimen (either the bundle or a single-rod) temperature within an acceptable (about 25°C) range.

The power supply is presently installed at the single-rod test facility, where it will be used in a planned series of heated shroud single-rod tests. A primary objective of this test series is to clarify the reasons for the greater deformation observed in bundle tests over that obtained in comparable single-rod tests. Six fuel-pin simulators were fabricated for testing in the next quarter.

Agreement was reached with NRC on conceptual design criteria and test conditions for the 8 × 8 (B-5) test, currently scheduled for mid-1980. The primary objectives of the test are to conduct a reasonably large bundle test under conditions that duplicate as nearly as possible those used in our single-rod and 4 × 4 bundle tests, so that the results can be considered representative of an infinite array and can be used for extrapolating and/or interpreting results from smaller test arrays. Design of the test equipment was nearly complete at the end of this reporting period.

Fabrication of the B-5 fuel-pin simulators was initiated. Approximately 75 simulators must be fabricated in order to obtain the required number of acceptable simulators for use in assemblying the test array. At the end of this reporting period, fuel simulator preparations (grooving for thermocouples, coating with ZrO_2, and characterizing axial heat generation by infrared scanning) were nearly complete, and six fuel pin simulators were assembled.

MULTIROD BURST TEST PROGRAM PROGRESS REPORT FOR APRIL–JUNE 1979

R. H. Chapman

ABSTRACT

Posttest examination and analysis of the B-3 test were essentially completed, and preliminary results are presented. These results confirm indications published earlier that deformation in the B-3 test was indeed greater than observed in the B-1 and B-2 tests. The greater deformation in B-3 is believed to be due to the lower heating rate used in the test (about 10°C/sec, compared with about 30°C/sec for the B-1 and B-2 tests).

Shakedown and demonstration tests of the new shroud and fuel-pin simulator temperature control systems were performed in the single-rod test facility with very encouraging performance. Some typical results are presented which indicate that the average temperature of the shroud can be controlled to within about 25°C of the average simulator temperature during both ramp and flat-topped transient heating tests of interest.

Conceptual design and tentative test conditions for the B-5 (8 × 8) bundle test were established, and detailed design of the test assembly was nearly completed. Fabrication of the fuel-pin simulators for the test array was initiated. The test is currently scheduled for May 1980.

---

1. INTRODUCTION

R. H. Chapman

The objectives of the Multirod Burst Test (MRBT) Program are (1) to delineate the deformation behavior of unirradiated Zircaloy cladding under conditions postulated for a loss-of-coolant accident (LOCA) and (2) to provide a data base that can be used to assess the magnitude and distribution of geometrical changes in the fuel-rod cladding in a multirod array and the extent of flow channel restriction that might result. Data are being obtained from single-rod and multirod experiments, both with and without electrical heating of the shroud surrounding the test arrays. The tests are designed to study possible effects of rod-to-rod interactions on ballooning and rupture behavior; a tentative test matrix was given in a

previous report.[1] Although the test matrix includes 11 × 11 test arrays, these will be held in abeyance until a definite need, based on the results of 4 × 4 and 8 × 8 test arrays, is established.

Approximately 53 single-rod burst tests have been conducted with a heating rate of about 28°C/sec; experimental details of these unheated-shroud tests and preliminary results have been reported routinely. (All published reports pertaining to this research program are listed in the Foreword of this report.) The data base covers a range of burst pressure from 770 to 19,150 kPa; the corresponding burst temperatures range from 1170 to 690°C. All the tests conducted prior to April 1977 were re-evaluated for validity, and the results were summarized in a previous report.[2] Readers using results obtained in this program should be aware that some of the earlier data points have been removed as a result of this reevaluation.

Four steady-state single-rod creep-rupture tests were conducted at about 760°C to determine whether large ballooning occurs over extended lengths of test specimens heated with internal fuel simulators. Test conditions were varied to cause failure in creep times of 49, 103, 162, and 250 sec. Two transient (about 28°C/sec) burst tests were conducted with the same internal fuel simulators for comparison. The initial conditions for the transient burst tests were adjusted to cause failure at approximately the same temperature as in the creep-rupture tests; the results of these tests were reported.[3]

Subsequently, two transient burst tests, using each of the same two fuel simulators, were conducted at nominal heating rates of 5 and 10°C/sec to bridge the span between the creep tests (approximately 0°C/sec) and the 28°C/sec transient burst tests. Initial pressure conditions for these tests were adjusted to cause failure at about 760°C for comparison. The results of these low-heating-rate tests were reported.[4]

The creep-rupture and the low-heating-rate tests were evaluated subsequently, and the results were reported in considerable detail in a recent topical report.[5]

Two transient (28°C/sec) burst tests were conducted to investigate the effect of steam flow rate on burst location. The steam flow rate in one test [Reynolds number (Re) about 800] was typical of that normally

employed in the single-rod tests; in the other, the flow (Reynolds number about 180) was comparable with that employed in the B-1 and B-2 bundle tests. The results of these tests have also been reported.[4]

All the above-discussed single-rod tests were conducted with an unheated shroud (ambient temperature of about 340°C) surrounding the fuel-pin simulator. Since this arrangement may cause significant heat losses from the simulator and enhance the circumferential temperature gradients therein, the deformation observed in these tests may be less than that expected in a fuel rod surrounded by others at about the same temperature.

Two 4 × 4 multirod tests, one (B-1) with and the other (B-2) without electrical heating of the shroud, have been conducted with a bundle heating rate of about 30°C/sec. Initial pressure conditions for these tests were selected to cause failure at about 860°C. Another 4 × 4 array (B-3) was tested with an electrically heated shroud using a bundle heating rate of about 10°C/sec; initial pressure conditions were selected to cause failure at about 760°C to provide a basis for comparison with the low-heating-rate single-rod tests.

Detailed results and interpretations of the B-1 and B-2 tests have been reported.[3,4,6] A topical report[7] interpreting the B-1 and B-2 water flow tests has been prepared and will be published in the near future. A data report[8] giving detailed results of the B-1 test without interpretation has been published. A similar report[9] on the B-2 test has been prepared and will be published in the near future. Quick-look results of the B-3 test have been reported,[6,10] and additional data are included in this report.

The substantial quantities of data accumulated in the MRBT program to date have all been obtained from unheated-shroud single-rod tests and from heated- and unheated-shroud 4 × 4 bundle tests in which (1) the shroud temperature at the time of burst was no closer than within about 80°C of the bundle temperature and (2) the rods were not confined sufficiently in their outward (radial) movement to simulate the radial restraint in a reactor core. The importance of closely simulating the thermal surroundings (thermal boundary) and confinement (deformation boundary) is not clear at this time, but the value of the data base will be increased by investigating these concerns in upcoming tests. One conclusion

that has remained valid throughout the testing is that, at a given deformation temperature level, temperature gradients determine deformation behavior: the more uniform the temperature distribution, the greater (and more uniform) the deformation. Therefore deformation results will be dependent on all factors that determine the temperature gradients, including the method and uniformity of heating, heating rate, heat losses to coolant and surroundings, and axial distribution of heat losses. Essentially all tests to date have been conducted at relatively low steam flow rates, and heat losses to coolant have been small but are still an important factor to consider.

Major emphasis of this report period was devoted to preparing for a new series of single-rod tests incorporating an electrically heated shroud, testing new shroud and fuel-pin simulator (FPS) temperature control systems, and preparing for an 8 × 8 bundle test (B-5) in which radial movement of the outer ring of rods will be restrained with a suitably positioned and supported reflective shroud. (The outer ring of rods may be regarded as sacrificial and as providing both a good thermal boundary and a good deformation boundary for the inner 6 × 6 bundle.) These and related activities are summarized in this report. Additional results of the bundle B-3 tests are also included.

2. PROGRAM PLANS AND ANALYSIS

2.1 Programmatic Activities

R. H. Chapman

Photographs of the B-3 bundle sections were analyzed to obtain strain profiles of each of the tubes and the total reduction in coolant flow area as a function of axial position. These results were presented at the Nuclear Regulatory Commission (NRC) Quarterly Cladding Research Review Meeting at the Idaho National Engineering Laboratory on June 25, 1979. The Annual Reactor Safety Research Information Exchange Meeting, involving United States, German, and Japanese representatives, was held at the same site after the Cladding Research Review Meeting, and MRBT staff personnel participated.

Representatives from several foreign and domestic research centers visited Oak Ridge during this reporting period to discuss matters of mutual interest. Our recent success with fabricating fuel-pin simulators, based on the use of cold-pressed boron nitride preforms, is apparently of widespread interest, and many of the visits were concerned with this technology.

Agreement was reached with NRC on conceptual design criteria and test conditions for the 8 × 8 bundle test (B-5), currently scheduled for mid-1980. The primary objectives of the test are to conduct a reasonably large bundle test under conditions that duplicate as nearly as possible those used in our single-rod and 4 × 4 bundle tests, so that the results can be considered representative of an infinite array and can serve as benchmarks for extrapolating and/or interpreting results from smaller test arrays.

These objectives are best satisfied by a test configuration that consists of an 8 × 8 array surrounded by a close-fitting, highly reflective, low-heat-capacity, unheated (i.e., without ohmic heating) shroud. The very thin shroud will be supported by, but thermally insulated from, a structure of sufficient strength to resist lateral movement of the outer ring of fuel-pin simulators. All the simulators will be identical in construction, pressurized to the same level, and heated at

the same rate. The outer ring of 28 simulators will serve both as guard heaters and as a deforming boundary for the inner 6 × 6 array, which will be representative of a very large bundle. Flow tests will be conducted on the burst bundle and on a reference bundle geometrically similar to it in its pretest condition.

The B-5 test will be a transient burst test, with the initial pressure selected to cause failure at about 760°C; the heating rate will be about 10°C/sec and the steam Reynolds number in the range of 150–250. These parameters permit comparison with the B-3 test.

A dolly-mounted power supply with associated control equipment for use in either the single-rod or the multirod test facility was placed in operation this quarter. This equipment will be in use at the single-rod facility for the next 12 to 15 months so that the effect of shroud temperature on cladding deformation can be investigated. The power supply and control equipment will also be used for heating the shrouds of future 4 × 4 bundle tests as desired to achieve test objectives.

2.2 Burst Temperature Correlation

R. H. Chapman

As reported earlier,[2,11] it was shown that burst temperature data obtained from transient heating tests at 28°C/sec can be correlated with burst pressure by the equation (obtained by a least-squares regression analysis)

$$T = 3907 - 0.0120P - \frac{10000P}{209 + 3.342P} ,$$

where T is the cladding temperature (°C) and P is the pressure (kPa) at the time of burst. Experimental data obtained[5] in a limited test series designed to scope the effect of heating rate on deformation suggested that the burst temperature correlation should also include a heating rate effect.

We have shown this to be the case by appropriate data from the literature. In particular, isothermal creep-rupture (about 100 sec hold

time) data of Hardy,[12] Leistikow,[13,14] and Hofmann[15] and very slow transient (0.3°C/sec) burst data of Emmerich et al.[16] were used for this purpose. These data were selected as being comparable with the creep-rupture scoping tests conducted[5] by this program.

The form of the above equation was modified to include the factor 1 + H, where H is the normalized heating rate. (For 0°C/sec heating, H = 0, and for 28°C/sec heating, H = 1.) The numerical constants in the equation were adjusted to give a good fit to the data for H = 0 and for H = 1, that is, they were adjusted to fit the data reported in refs. 12–16 and in refs. 2 and 11 respectively. The resulting equation is

$$T = 3960 - \frac{0.024P}{1 + H} - \frac{10000P}{100(1 + H) + 3.28P} ,$$

where T is burst temperature (°C), P is burst pressure (kPa), and H is the normalized (dimensionless) heating rate. Figure 2.1 compares the equation with the experimental data. The limited data from ref. 5 (not used in determining the numerical constants) are also included in the plot as a test

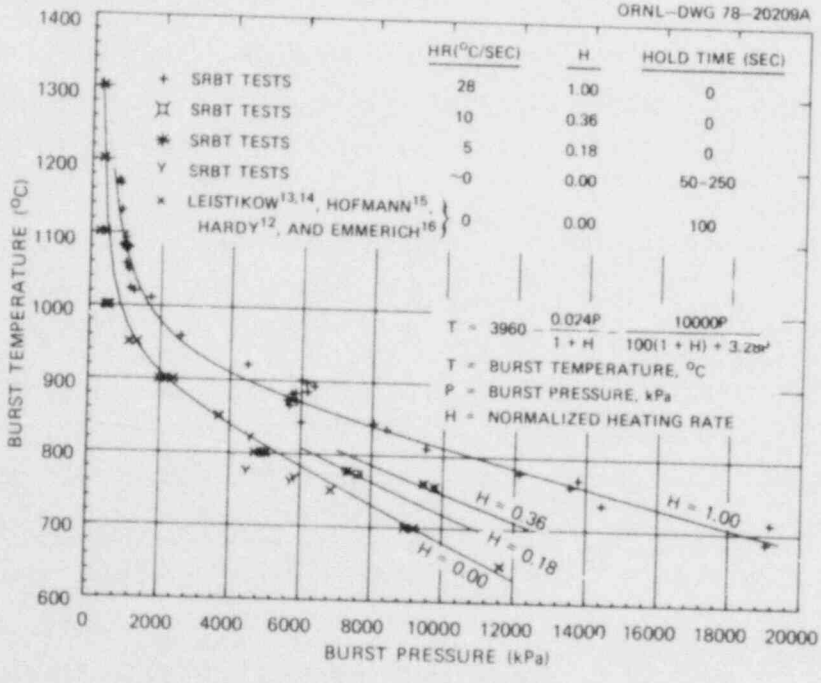

Fig. 2.1. Correlation of single-rod burst temperature data with burst pressure and heating rate.

of how well the correlation predicts the results for other heating rates. As is evident from the figure, the correlation predicts the ref. 5 data quite well.

This attempt to correlate burst temperature with both heating rate and burst pressure gave very encouraging results. We plan to collect data from the literature for a variety of heating rates and to use this broad data base in optimizing the coefficients. Also, the correlation will be rewritten in terms of burst stress to increase the range of applicability.

2.3 Additional B-3 Test Results

R. H. Chapman D. O. Hobson*

Further examination and analysis of the B-3 test have been performed, and the results are summarized herein. These results supplement (and replace in some instances) those reported[6,10] earlier.

It will be recalled that the B-3 fuel pin simulators incorporated the fuel simulators from the B-1 test assemblies in the same positions and relative orientations. This permits comparison of the two tests without considering differences in fuel simulator characteristics. The B-3 heating rate was 9.5°C/sec (30.1°C/sec for B-1), and the bursts occurred at about 764°C (865°C for B-1). Inlet steam conditions in the two tests were essentially the same, namely, Re ≈ 263 in B-3 and 250 in B-1. The shroud was electrically heated in both tests; however, due to technical problems, the shroud heating rate was less than that of the bundle in the tests (7.1°C/sec for B-3 and 20.0°C/sec for B-1). The lower shroud heating rate resulted in the B-3 bundle temperature being about 80°C higher than that of the shroud during the time deformation was taking place. Similarly, the B-1 bundle temperature was about 140°C higher than that of its shroud.

Table 2.1 gives a computer printout (with data evaluation comments added) of the initial and burst conditions for each of the tubes in the B-3 test. This printout was compiled from the data tape and incorporates the appropriate calibration corrections for the various transducers. This

---

*Metals and Ceramics Division.

Table 2.1. Summary of B-3 burst test results

POWER-ON TIME 15:20:18.63 POWER-OFF TIME 15:21: 5.82 POWER WAS ON 47.19 SECONDS

ROD NO.	INITIAL CONDITIONS					MAXIMUM PRESSURE DIFFERENTIAL (KPA)	APPROXIMATE BURST CONDITIONS					BURST TIME (SEC)
	DIFFERENTIAL PRESSURE (KPA)	TEMPERATURES (DEG C) TE-1	TE-2	TE-3	TE-4		DIFFERENTIAL PRESSURE (KPA)	TEMPERATURES (DEG C)[a] TE-1	TE-2	TE-3	TE-4	
1	11584.8	325.3	325.7	329.5	329.9	12060.9	9407.2	754.6	736.7	750.9	771.2	45.89
2	11598.9	328.1	329.9	330.4	330.4	12066.6	8825.2	748.0	778.8	742.2	741.0	45.89
3[b]	11619.7	330.9	325.7	329.9	329.5	12133.0	5112.5[b]	473.7[b]	405.8[b]	752.7[b]	682.1[b]	43.84[b]
4	11631.7	328.5	330.4	330.4	329.9	12132.3	9091.2	760.8	765.5	767.4	735.8	47.44
5	11585.8	326.7	330.4	329.0	329.9	12057.3	9477.9	752.3	763.2	763.6	759.8	46.29
6	11580.3	325.7	329.0	330.9	330.4	12057.2	9155.5	757.5	769.8	766.9	769.3	46.19
7[c]	11725.4[c]	331.8	325.3	330.4	330.4	11753.3[c]	11357.3[c]	724.1	741.9	753.7	738.7	44.89[c]
8	11653.5	326.2	328.1	329.9	329.0	12178.8	9107.9	749.0	754.6	756.5	745.7	46.19
9	11535.9	324.3	329.9	330.4	330.9	12035.9	9106.5	754.2	750.4	785.4[d]	730.6	45.74
10	11577.1	332.3	329.5	329.9	329.9	12073.2	9393.0	739.1	774.5	760.8	767.9	45.79
11	11611.0	326.7	329.0	330.9	330.4	12132.4	9626.2	750.4	738.4	742.5	775.0	45.14
12	11683.5	330.4	329.9	329.9	321.5[e]	12192.5	9754.0	747.5	760.8	745.3	699.7[e]	45.99
13	11571.9	331.3	329.5	329.5	329.9	12073.2	10246.6	737.2	763.3	754.6	748.3	44.65
14	11611.9	326.2	324.3	329.5	329.5	12104.2	9492.1	714.2	727.8	755.6	769.3	45.59
15	11651.2	329.5	329.5	328.1	329.5	12168.0	9202.6	742.8	749.5	750.9	750.4	45.44
16	11680.7	325.3	330.4	329.5	330.4	12190.8	9702.4	740.5	747.1	742.9	730.4	45.79

[a] Underlined value is burst temperature based on premise that maximum value is minimum possible burst temperature.

[b] Rod 3 partially depressurized due to a small leak during test and its behavior was abnormal.

[c] Rod 7 developed a leak prior to test; this rod was tested essentially at constant pressure due to attempt to compensate for leak.

[d] TE 9-3 was known to be detached from Zircaloy prior to test, causing a high reading; TE 9-1 reading was selected as burst temperature.

[e] TE 12-4 had very slow response on both heatup and cooldown transients, and its readings should be ignored.

explains why the pressure and temperature data are shown to one more significant figure than the data warrant. The burst temperature pressure data are plotted and compared in Fig. 2.2 with predicted values obtained from the single-rod correlation discussed in the preceding section. The B-3 data point to the left of the H = 0.0 (i.e., isothermal creep rupture) curve is for tube 3, which, as reported earlier,[6] failed under essentially isothermal creep-rupture conditions. The figure also compares the B-1 and B-2 data with the single-rod correlation. The two data points above the H = 1.0 curve (at about 925°C) are for tubes that partially depressurized prior to the tests.[3]

The bundle was sectioned at a number of axial locations, and the previous report[10] showed photographs and approximate strain data for the sections containing tube bursts. Enlarged (about 5×) photographs of all the sections have been analyzed to obtain geometrical data that can be used to describe the deformation in the bundle. Table 2.2 gives the strain in each tube at each of the axial locations; these data supersede those presented in the previous report.[10]

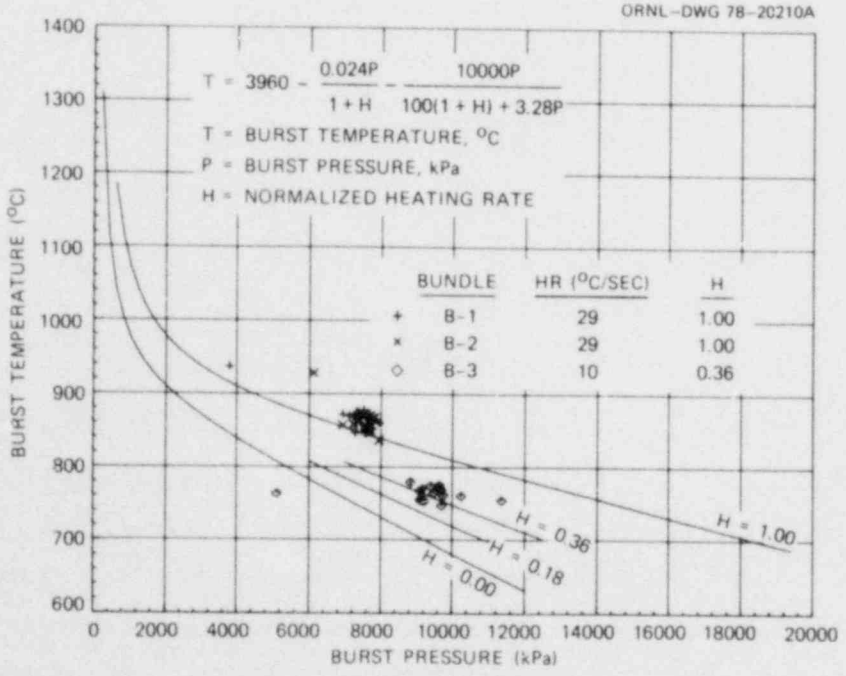

Fig. 2.2. Comparison of bundle burst data with single-rod correlation relating burst temperatures to burst pressure and heating rate.

Table 2.2. Strain in B-3 tubes in percent

ELEVATION (cm)	TUBE NO.															
	1	2	3	4	5	6	7	8	9	10	11	12	13	14	15	16
0.0	0.5	0.6	0.6	0.3	0.3	0.5	0.0	-0.1	0.4	-0.0	-0.1	0.2	0.5	0.3	0.4	0.4
1.8	2.4	1.4	3.5	2.3	1.5	2.3	1.7	0.9	1.4	2.1	2.7	3.5	4.5	2.4	0.8	1.5
3.5	6.0	7.5	10.2	7.4	5.1	8.6	8.6	7.3	6.7	11.0	7.1	7.2	6.4	7.1	6.4	5.9
5.0	6.9	14.0	12.4	9.4	6.7	11.8	12.5	11.6	9.5	15.2	9.1	7.8	5.7	9.1	13.8	8.0
6.7	6.2	13.4	8.7	8.6	6.7	9.7	11.4	10.2	9.0	12.6	8.5	6.3	5.0	8.0	13.3	7.1
8.7	2.7	6.5	3.6	4.5	3.6	4.5	4.5	4.0	3.7	5.0	3.5	2.5	2.5	2.8	5.4	2.5
11.6	5.3	6.0	5.6	5.0	5.2	6.1	7.2	5.4	4.7	7.0	5.5	5.0	6.7	5.1	5.8	4.8
13.4	13.1	13.9	11.5	12.7	11.0	14.3	17.4	13.5	11.0	17.7	14.6	13.9	17.9	12.9	15.6	13.1
15.3	16.3	23.0	16.1	21.5	18.6	22.8	21.5	18.4	16.9	25.2	16.9	18.4	28.5	18.7	35.8	22.2
17.2	16.3	23.0	19.4	27.8	23.9	24.5	23.4	19.2	19.2	26.7	23.4	17.9	18.9	20.9	49.1	28.9
19.0	18.5	26.7	20.5	45.7	23.0	27.4	25.7	23.5	24.8	29.5	33.5	17.8	13.5	26.7	53.6	30.7
20.7	17.2	31.6	18.5	60.1	22.3	32.5	28.7	25.9	28.8	37.1	34.1	18.9	11.2	25.7	56.9	32.5
22.5	19.1	30.9	18.2	39.5	28.7	36.5	31.5	26.9	29.3	49.9	33.9	23.8	11.5	24.4	51.5	45.9
24.2	20.2	34.9	22.3	33.7	38.6	36.4	34.6	27.9	32.8	52.7	42.4	31.4	14.5	29.9	43.9	57.5
25.6	20.6	41.3	28.1	37.1	52.1	38.6	40.2	29.9	50.4	49.3	58.4	34.0	19.3	41.8	34.7	44.7
26.8	20.9	44.0	31.3	40.3	64.7	50.5	37.1	26.9	62.8	42.8	47.9	30.8	24.1	40.5	27.4	32.2
28.2	21.9	40.5	30.4	39.3	44.8	58.8	30.2	23.6	51.8	34.0	30.2	28.6	33.4	33.7	24.6	27.8
29.7	21.4	36.9	27.7	31.7	39.5	47.3	26.4	23.3	37.6	28.3	23.2	27.8	52.6	27.2	30.0	27.4
31.3	17.4	39.3	24.9	24.7	28.2	28.3	25.8	24.3	32.8	23.5	21.3	28.9	41.6	24.3	43.2	24.5
32.6	15.5	44.5	24.2	22.2	24.6	23.8	29.9	25.7	29.2	22.6	20.9	29.2	26.4	21.9	63.1	21.3
33.8	12.6	44.9	24.0	22.7	21.3	22.8	31.4	24.8	24.7	21.2	20.2	27.9	19.3	18.6	54.0	21.1
35.0	13.5	45.5	30.1	25.9	22.4	25.4	33.7	24.4	23.3	21.2	19.9	24.8	18.1	18.0	48.1	22.6
36.1	13.3	44.4	49.7	28.6	22.5	25.3	33.9	25.7	20.8	19.3	19.7	21.2	18.5	18.0	35.4	24.7
37.5	14.0	54.1	73.9	31.3	22.2	24.6	35.6	31.7	18.5	19.0	20.8	21.1	23.5	18.9	32.4	26.1
39.2	15.0	75.8	45.4	30.8	20.4	24.8	39.3	40.8	21.3	21.4	20.6	22.6	33.5	22.4	33.5	24.4
40.8	25.6	67.9	27.9	31.0	24.4	28.8	43.4	46.5	31.6	28.8	21.4	24.4	31.6	25.5	29.8	24.0
42.4	24.9	44.9	29.6	30.8	28.3	29.7	40.8	55.4	44.1	29.4	20.1	29.0	20.9	25.8	27.0	25.3
44.0	24.3	40.5	35.1	32.9	29.1	28.9	43.6	75.1	58.9	25.9	20.1	32.2	18.3	28.1	28.4	24.2
45.2	27.6	41.9	34.4	35.0	31.8	30.0	47.3	77.2	58.7	26.8	21.4	35.3	17.8	28.0	29.3	21.1
46.8	30.0	43.9	36.0	35.7	37.8	37.3	61.6	58.0	50.1	29.9	23.0	46.4	17.5	25.4	28.5	19.4
48.3	28.3	35.6	39.5	38.4	39.7	38.6	48.8	37.4	39.1	31.2	20.7	47.1	14.7	20.9	24.0	19.8
50.0	37.5	32.7	51.4	33.7	37.3	36.3	34.9	30.1	37.0	33.3	21.3	36.9	15.4	21.6	21.3	20.3
51.6	48.1	34.3	39.0	25.0	27.7	33.2	32.2	27.1	32.7	33.2	20.6	26.0	13.9	21.1	21.3	18.7
52.9	46.7	35.5	27.8	21.8	24.2	30.7	29.0	23.2	30.5	30.9	19.6	20.5	14.3	20.7	22.2	17.4
54.3	27.5	28.6	20.6	21.2	21.6	26.7	24.2	21.4	25.4	25.5	18.6	17.8	11.6	18.2	20.9	16.0
55.8	19.8	22.8	17.8	19.4	21.2	22.4	21.0	22.4	21.6	22.0	17.6	16.4	11.3	17.2	18.4	15.4
57.5	17.9	19.7	16.0	18.5	19.1	17.3	20.2	23.9	18.7	17.9	16.5	14.3	11.1	17.1	15.2	13.2
59.2	17.5	17.5	14.0	19.3	15.1	15.2	19.4	20.4	15.3	16.4	15.3	12.4	10.4	16.4	13.7	11.2
61.0	13.4	12.1	10.5	13.6	10.8	11.7	12.4	12.4	10.4	12.0	10.5	9.1	8.5	11.6	10.6	8.4
62.9	4.8	4.7	4.2	4.1	4.4	4.6	4.6	3.8	3.7	4.4	3.8	3.2	3.5	3.9	4.2	3.2
65.8	5.6	5.6	4.9	4.0	4.8	5.3	5.1	5.1	5.1	4.4	4.7	2.9	3.3	3.9	4.0	3.2
67.8	14.7	11.7	10.9	10.9	9.9	12.0	10.7	11.6	9.1	8.6	10.8	7.8	5.0	8.4	7.4	7.9
69.5	26.1	16.3	16.0	17.5	15.4	17.7	13.3	16.6	13.3	12.9	15.0	12.5	7.7	14.5	10.6	13.2
71.2	25.7	18.6	17.3	19.9	15.1	16.7	13.0	17.4	13.1	11.1	14.9	10.5	5.6	15.5	9.3	12.1
72.9	32.6	21.9	17.2	23.8	15.7	17.4	14.2	18.4	15.2	12.4	17.0	11.1	6.3	17.9	10.9	12.8
74.6	30.1	22.4	16.5	31.3	16.1	17.4	15.4	17.6	15.8	13.2	16.9	12.9	8.0	18.8	12.0	13.4
76.4	24.5	19.4	14.5	36.5	13.5	16.1	13.7	16.4	13.1	11.0	15.1	13.8	7.6	17.3	10.7	11.9
78.2	22.9	19.3	14.6	35.1	12.5	16.6	14.0	18.6	13.8	11.0	15.9	14.3	8.5	17.5	10.1	11.8
80.1	20.2	18.4	13.8	28.4	11.5	18.2	13.1	15.3	14.0	10.6	15.5	12.3	8.2	17.6	10.6	10.2
82.0	16.7	17.0	12.1	20.1	10.9	17.3	11.0	10.7	11.4	9.4	12.5	10.6	6.9	13.6	10.6	9.3
83.8	12.9	15.4	9.0	11.6	10.1	12.0	8.9	8.3	11.0	8.8	9.9	9.6	7.0	10.4	10.0	9.1
85.6	10.8	11.0	6.8	7.5	7.9	7.5	5.9	6.3	9.2	6.6	6.9	6.4	6.1	6.7	7.2	8.6
87.5	6.8	4.8	3.7	4.7	3.6	4.2	3.6	3.9	4.1	3.9	4.1	2.0	2.9	3.4	4.6	5.1
89.5	2.7	1.5	1.4	2.4	0.8	1.5	0.9	1.0	0.4	0.6	0.8	0.3	0.2	0.5	1.4	1.0
91.5	1.5	1.2	1.0	1.0	0.5	0.8	0.7	0.9	0.8	1.0	0.7	0.4	0.6	0.4	0.8	0.1

Tube deformation profiles are shown in Figs. 2.3–2.18. The pre-test infrared characterization scan of the fuel simulator and the axial location of the thermocouple for the respective fuel-pin simulators are also shown for reference purposes. The length of the tube burst is noted by the spacing of the arrows denoting "burst zone"; these measurements were obtained by use of a Boroscope prior to casting the bundle in an epoxy matrix for sectioning.

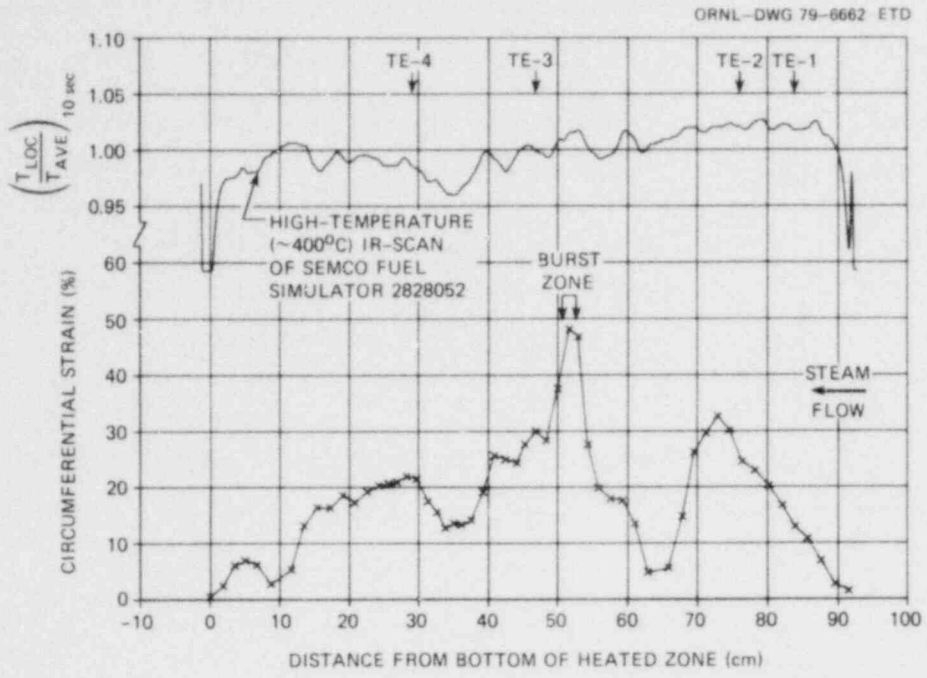

Fig. 2.3. Deformation profile of rod 1 in B-3 test.

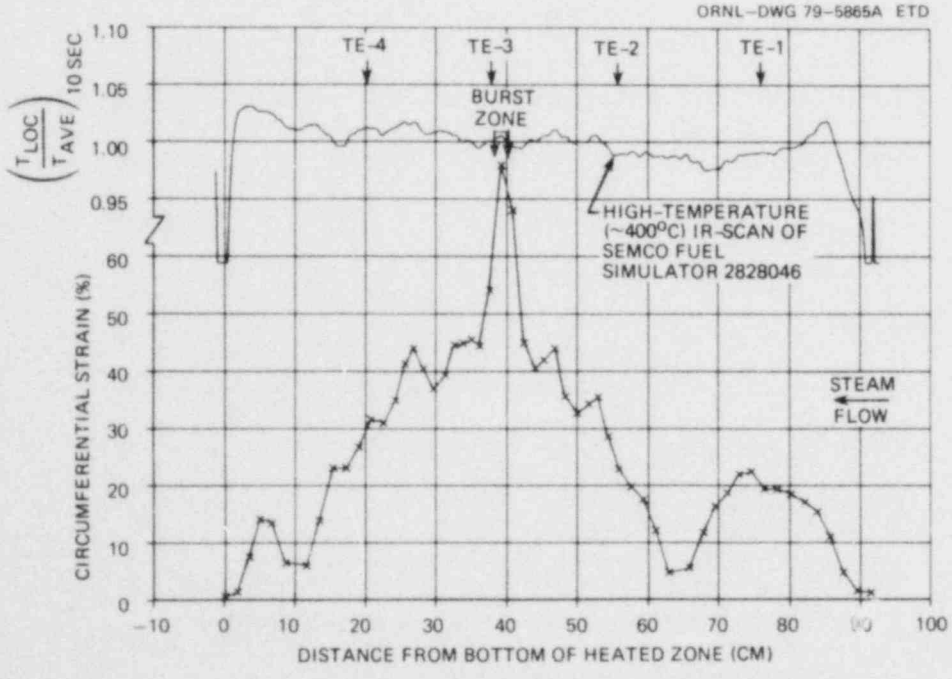

Fig. 2.4. Deformation profile of rod 2 in B-3 test.

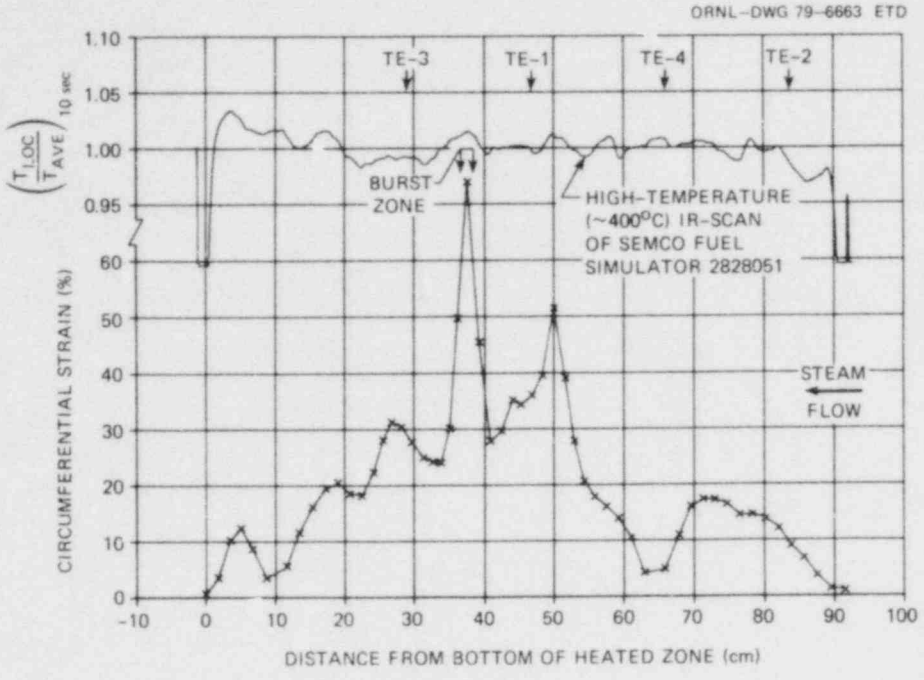

Fig. 2.5. Deformation profile of rod 3 in B-3 test.

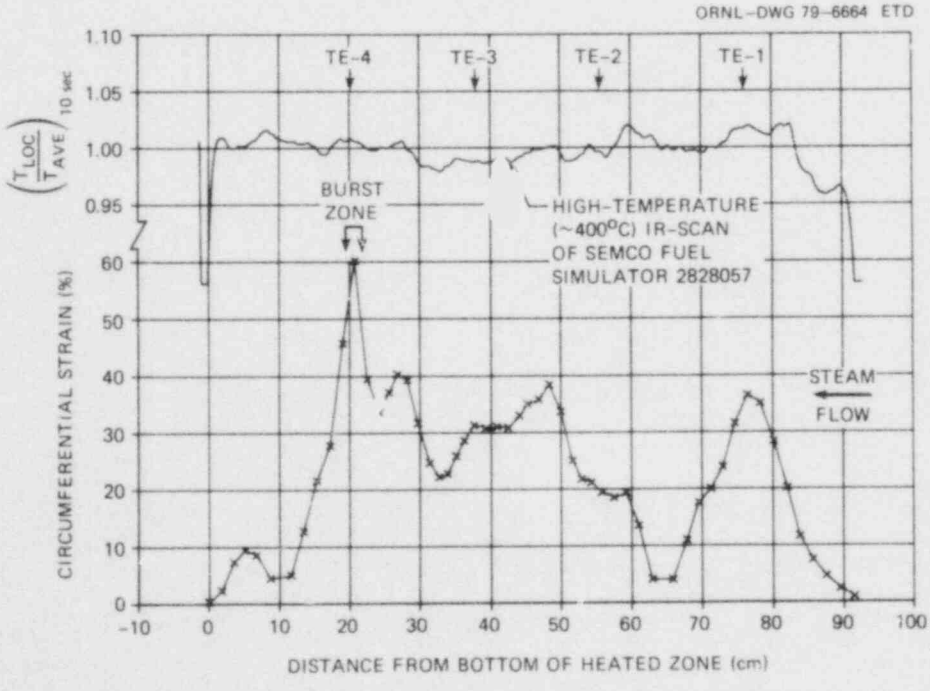

Fig. 2.6. Deformation profile of rod 4 in B-3 test.

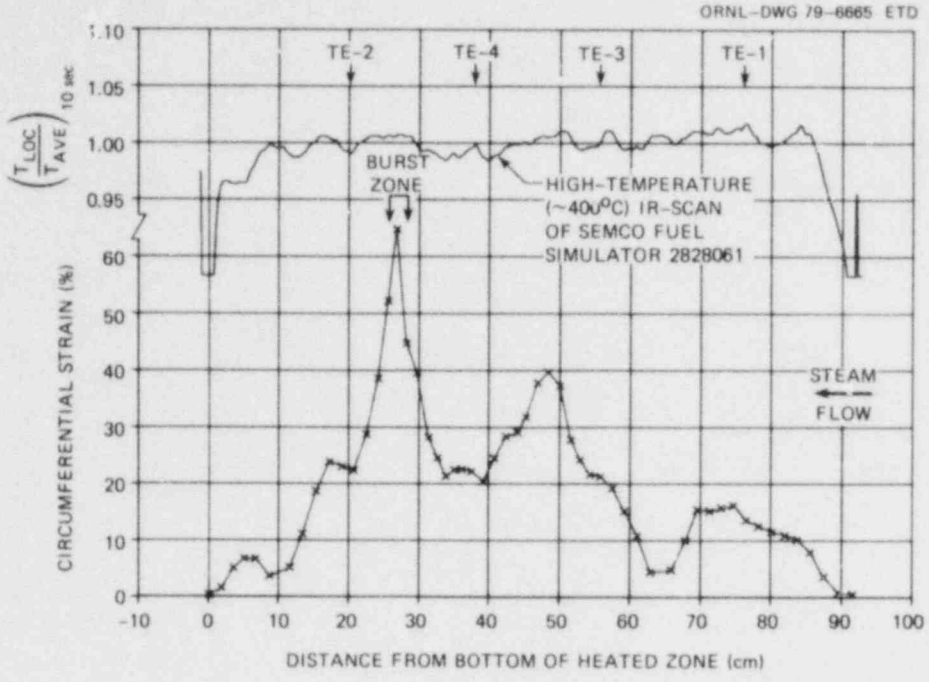

Fig. 2.7. Deformation profile of rod 5 in B-3 test.

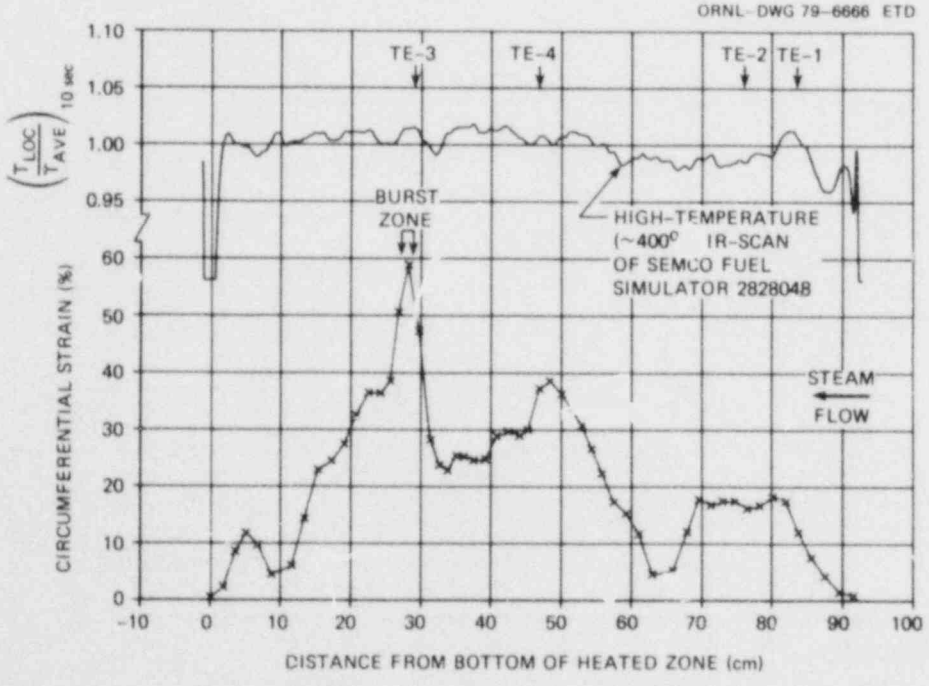

Fig. 2.8. Deformation profile of rod 6 in B-3 test.

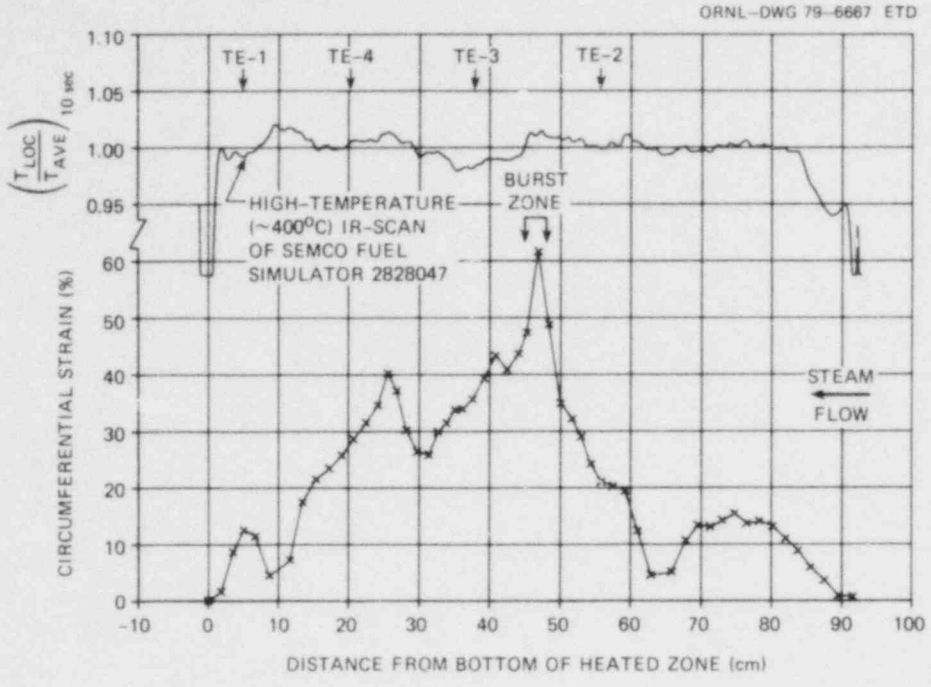

Fig. 2.9. Deformation profile of rod 7 in B-3 test.

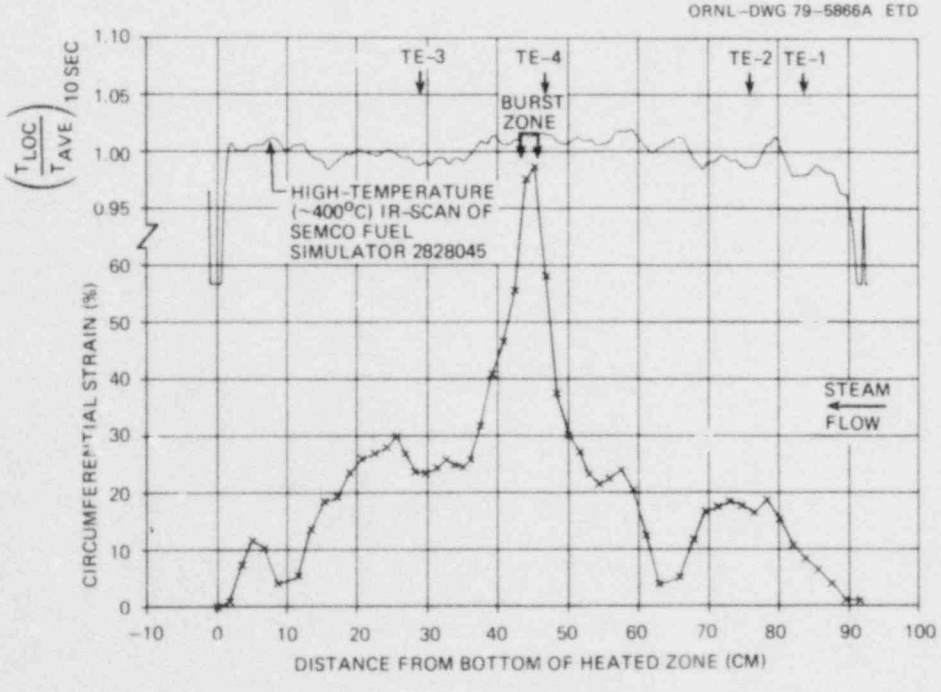

Fig. 2.10. Deformation profile of rod 8 in B-3 test.

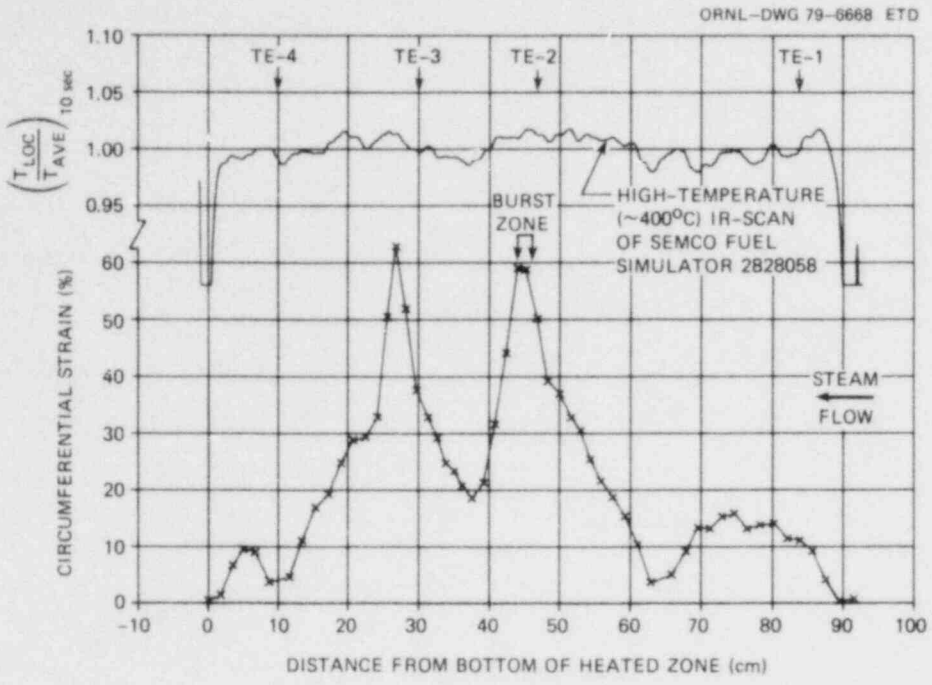

Fig. 2.11. Deformation profile of rod 9 in B-3 test.

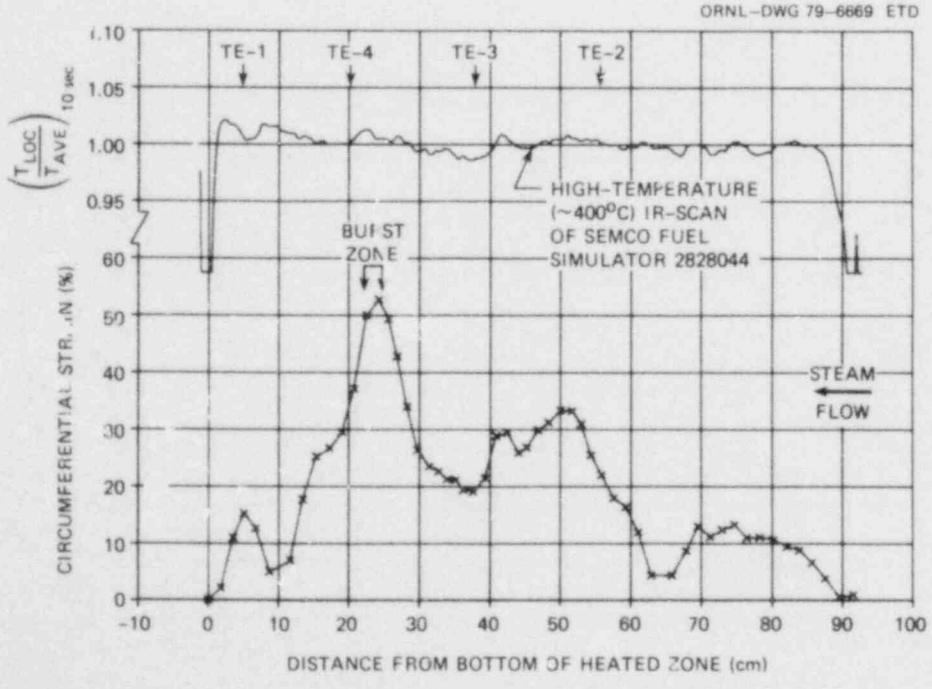

Fig. 2.12. Deformation profile of rod 10 in B-3 test.

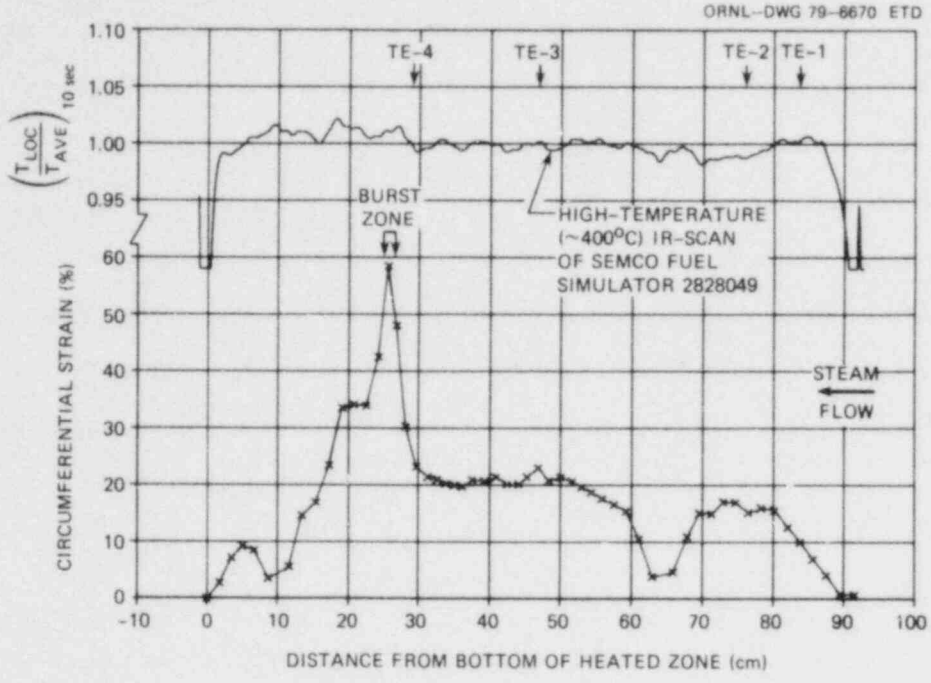

Fig. 2.13. Deformation profile of rod 11 in B-3 test.

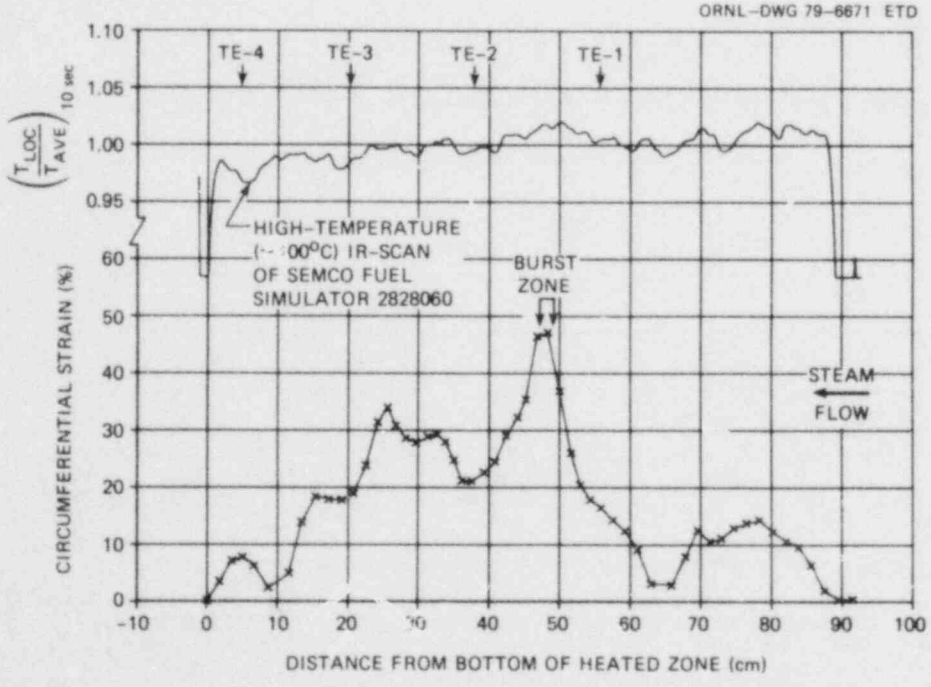

Fig. 2.14. Deformation profile of rod 12 in B-3 test.

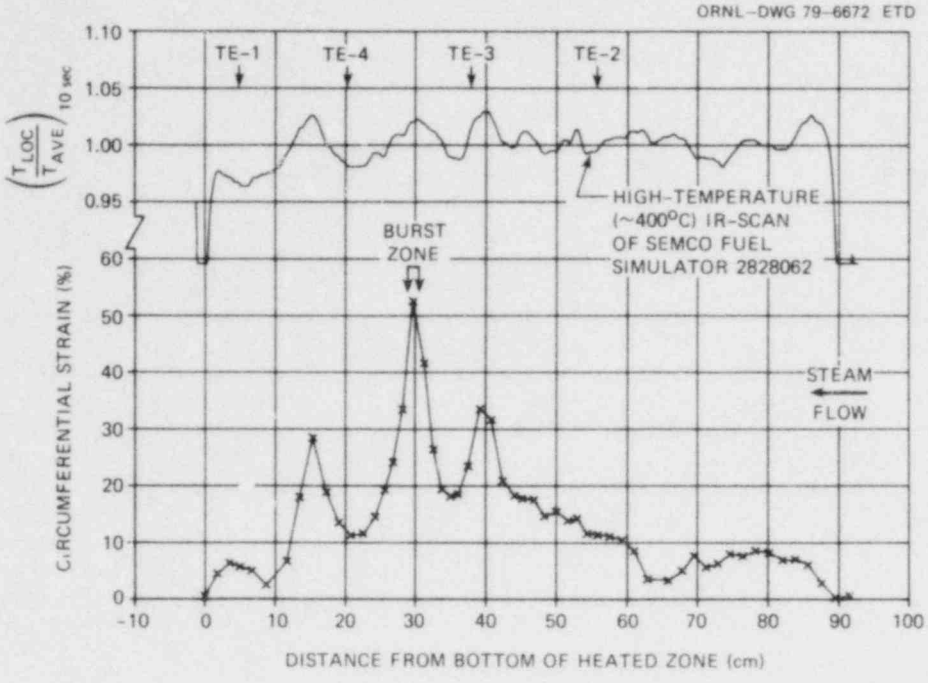

Fig. 2.15. Deformation profile of rod 13 in B-3 test.

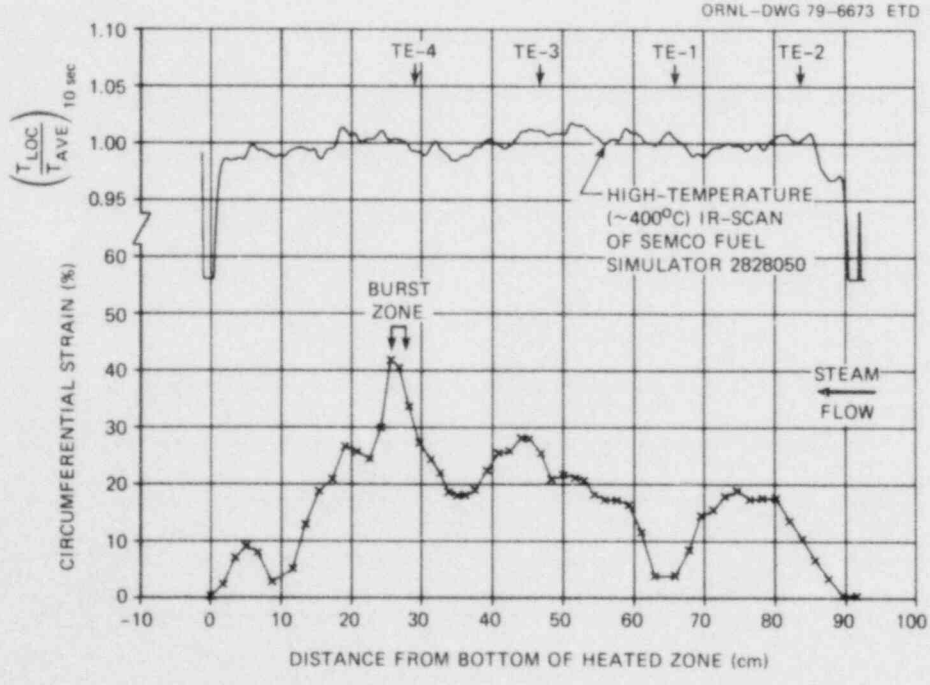

Fig. 2.16. Deformation profile of rod 14 in B-3 test.

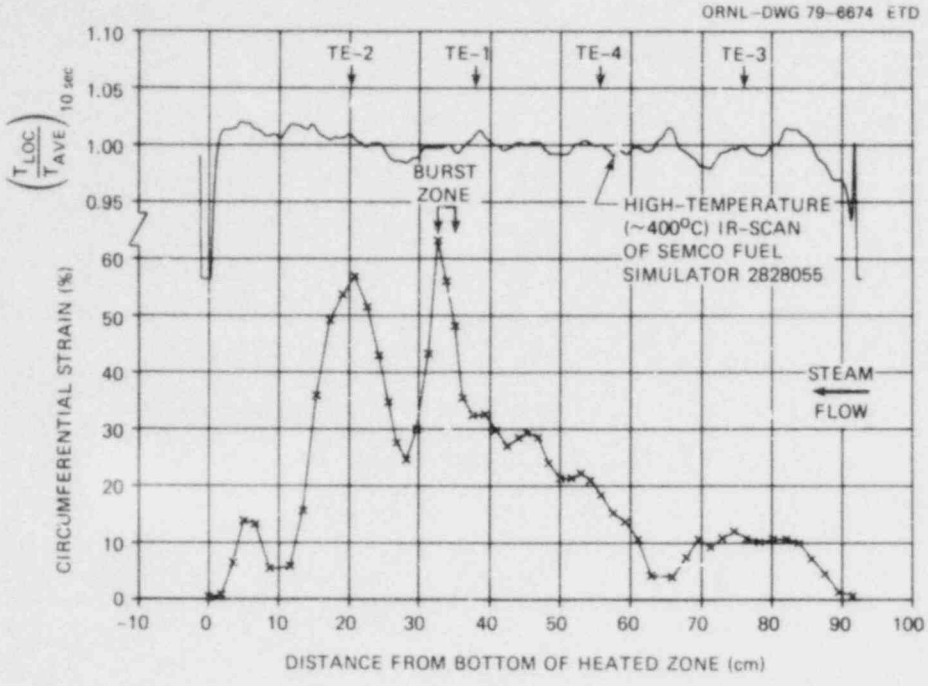

Fig. 2.17. Deformation profile of rod 15 in B-3 test.

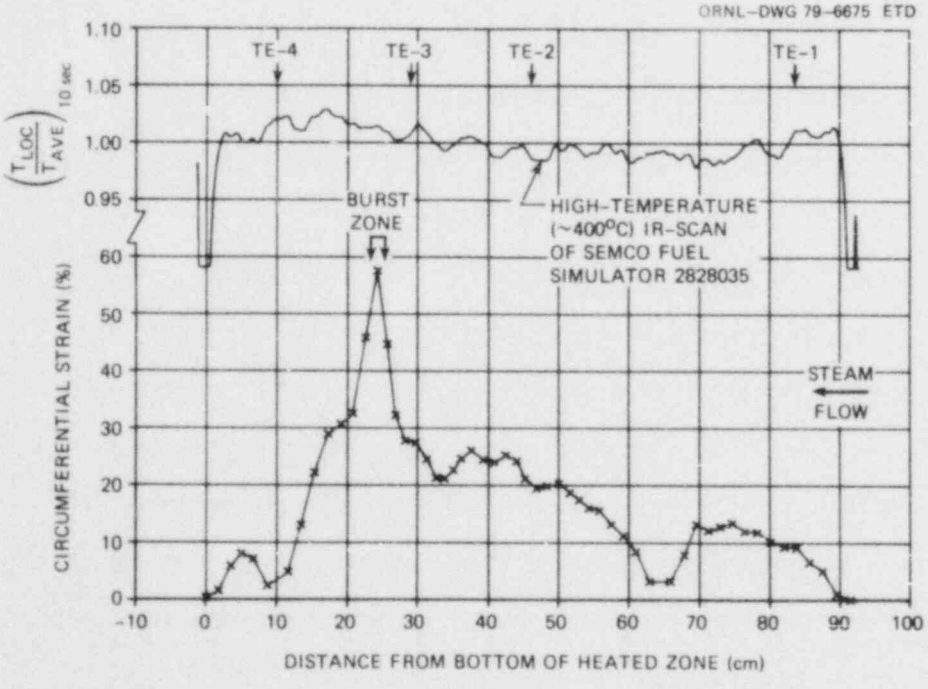

Fig. 2.18. Deformation profile of rod 16 in B-3 test.

All the deformation profiles have certain characteristics, more or less independent of the characteristics of the individual fuel simulators. These include strains of 3 to 8% in the region of the grids (centered about the 10- and 66-cm elevations) and maximum strains of 5 to 15% in the region between the bottom of the heated zone and the lower grid. Most tubes exhibited maximum strains of 10 to 20% in the region between the upper grid and the top of the heated zone. Strain in this region was influenced by the cooling effect of the incoming steam.

The deformation profiles and tube burst locations correlate rather well with the pretest infrared characterization scans considering the facts that (1) the grids have a strong restraining effect, (2) circumferential temperature gradients are known to exist in the fuel simulators, and (3) the characterization scans are for a single angular orientation. The maximum burst strain (77%) occurred in tube 8 and the minimum (42%) in tube 14. Figure 2.19 compares the B-3 burst strains with the B-1 burst strains and with single-rod data obtained with an unheated shroud.

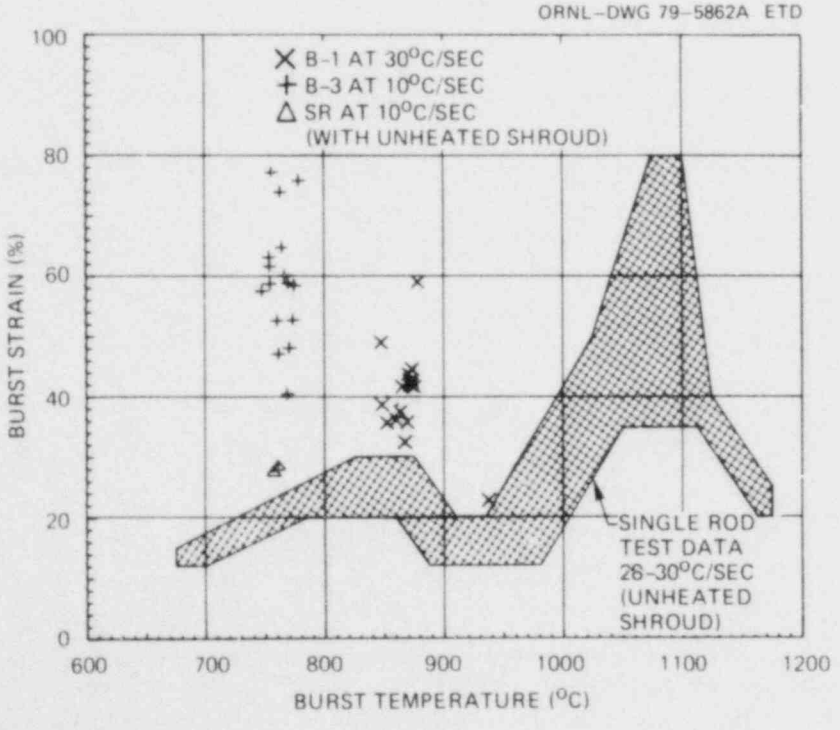

Fig. 2.19. Comparison of B-3 burst strains with B-1 and single-rod test data.

The tube bursts are shown in a composite layout, Fig. 2.20, in which the tube-to-tube pitch is greatly exaggerated for clarity. The quick-look burst orientations presented earlier[6] have been reevaluated to define the angle of the burst more precisely. This was done by examination of the photographs of the bundle sections in the vicinity of the bursts to ascertain wall thinning. Based on this examination, our best estimates of the angular orientations are given (with axial locations) in Table 2.3 and are shown in Fig. 2.21.

Axially extended ballooning is of concern in thermal hydraulic analyses of deformed bundles. While this characteristic has no precise definition, we arbitrarily define it to mean more than 32% strain over a tube length (L) equal to 20 (original) tube diameters (D). This definition derives from the fact that for the tube diameter and tube-to-tube pitch used in our tests, 32% uniform strain on each tube will produce contact on adjacent tubes. The 20L/D length is a figure of merit for flow disturbances. Figure 2.22 is a plot of those regions of the B-3 tubes which

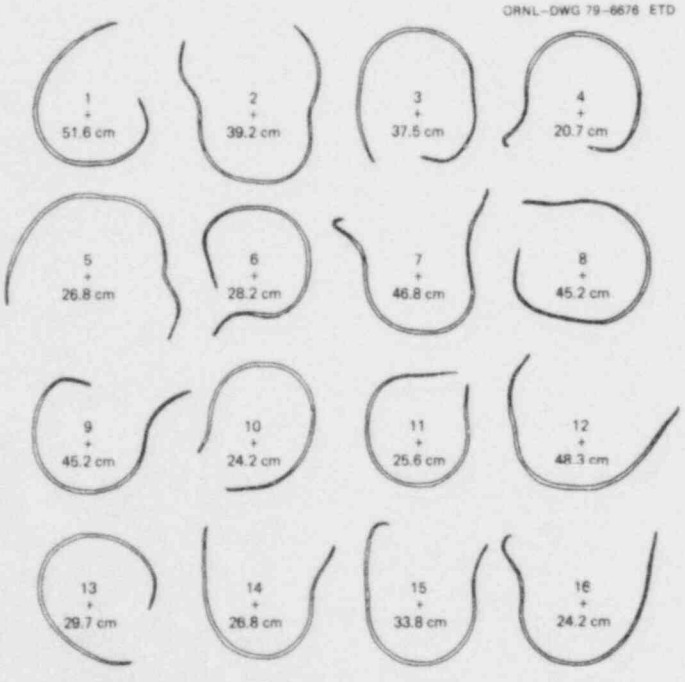

Fig. 2.20. Composite layout of tube bursts in B-3 test. Tube-to-tube pitch greatly exaggerated for clarity. Axial locations of bursts are noted.

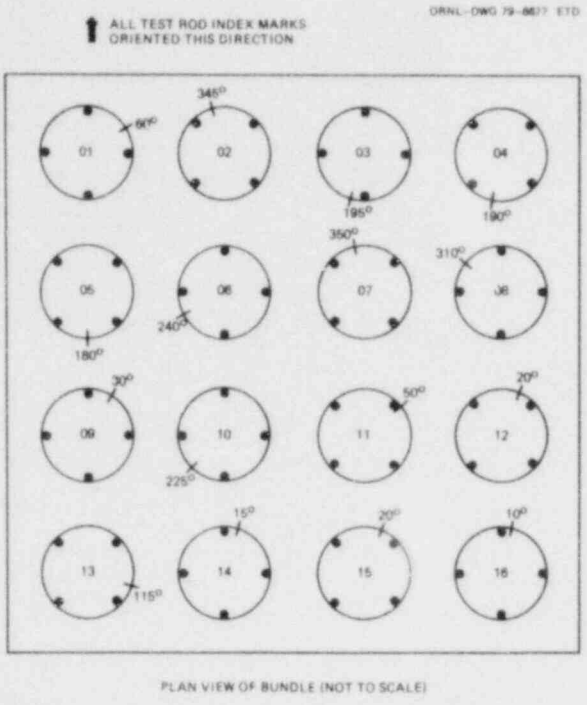

Fig. 2.21. Angular distribution of bursts in B-3 test.

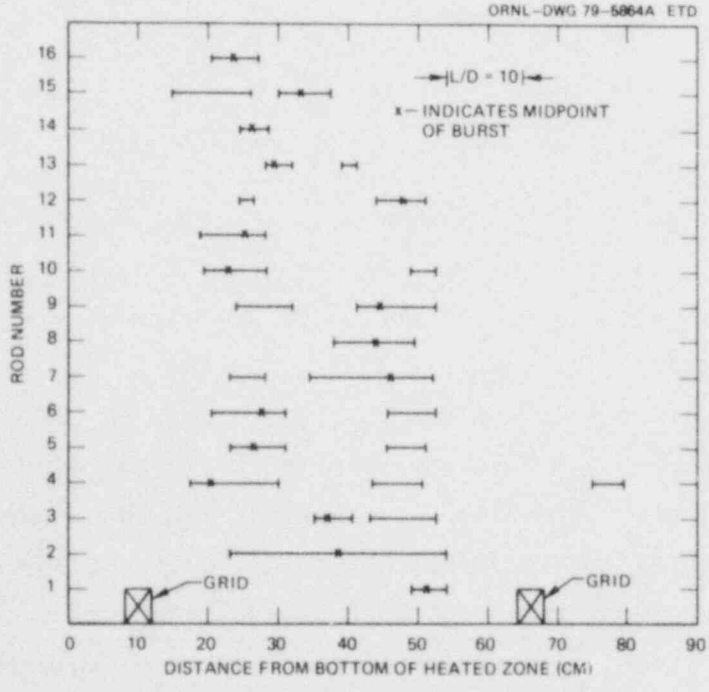

Fig. 2.22. Portions of B-3 tubes with more than 32% circumferential strain.

Table 2.3. Location of bursts in B-3 test

Simulator No.	Burst location	
	Axial[a] (cm)	Angle[b] (deg)
1	51.2	60
2	38.9	345
3	37.1	195
4	20.3	190
5	26.6	180
6	27.7	240
7	46.1	350
8	44.1	310
9	44.7	30
10	23.0	225
11	25.3	50
12	47.8	20
13	29.4	115
14	26.3	15
15	33.4	20
16	23.8	10

[a] Elevation above bottom of heated zone.

[b] Measured clockwise looking down on top of bundle.

exceeded 32% strain. As is evident from the figure, tube 2 experienced strains greater than this value over a length of approximately 28.5 (original) tube diameters; hence, by the above definition, axially extended ballooning was observed on this tube.

Another characterization of tube deformation is the volume increase over the heated length. This parameter is believed to be more closely related to flow resistance (B-3 experimental flow data were reported[6] earlier) than burst strain, since the volume increase takes into account deformation along the length of the tube, while burst strain is a highly localized parameter. The volume increase was calculated for each of the tubes by use of the strain data given in Table 2.2, assuming that the tube cross sections are circular. The average strain was calculated from the

volume increase by assuming the volume increase to be uniformly distributed along the heated length. The results of this analysis are given with other characteristics of the test in Table 2.4. Figure 2.23 compares the B-3 heated-length volume increase data with B-1, B-2, and single-rod test data. As is evident in the figure, the B-3 data are not significantly greater than the B-1 and B-2 data, even though the burst strains were greater (see Fig. 2.19).

As is evident from the above discussion and the deformation profiles for the individual tubes (Figs. 2.3–2.18), significant deformation was observed at a number of points. However, the total expansion for all the tubes at any cross section is much more important, since it determines the restriction in the coolant-channel flow area.

One method for calculating the restriction in the coolant-channel flow area is to consider unit cells centered about the open space between fuel rods; an alternative method considers unit cells centered about the fuel rods. Obviously, both methods give the same result for infinite arrays, but for small test arrays, different results will be obtained. We

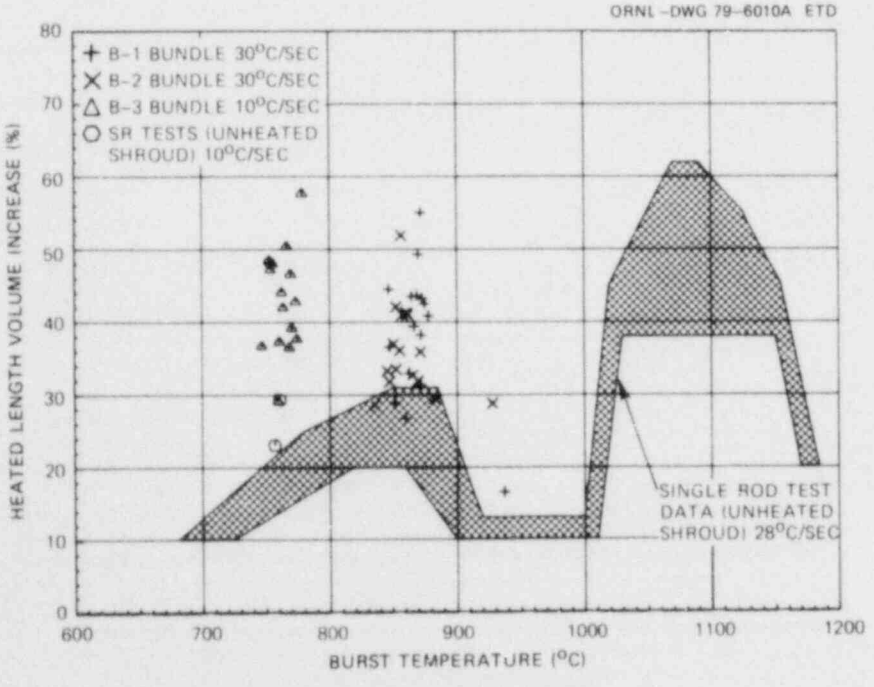

Fig. 2.23. Comparison of volume increase of B-3 tubes with B-1, B-2, and single-rod test data.

Table 2.4. Characterization of B-3 tube failures

Rod No.	Initial gas volume[a] (cm^3)	Approximate burst condition			Fractional[b] pressure decrease	Fractional[c] volume increase	Volume increase[d] of tube over heated length (%)	Average strain[e] (%)
		Pressure (kPa)	Temperature (°C)	Strain (%)				
1	49.0	9605	771	48	1.21	1.67	39.1	18
2	51.5	8825	779	76	1.31	1.95	57.6	26
3[f]	49.7	5115[f]	763[f]	74[f]	2.27[f]	1.76[f]	44.0[f]	20[f]
4	49.9	9090	767	60	1.28	1.86	50.3	23
5	51.1	9480	764	65	1.22	1.70	41.9	19
6	50.7	9155	770	59	1.27	1.79	46.5	21
7[g]	49.7	11355[g]	754[g]	62[g]	1.03[g]	1.82[g]	48.1[g]	22[g]
8	49.3	9105	75[illegible]	77	1.28	1.83	47.9	22
9	49.5	9105	754	59	1.27	1.81	47.1	21
10	50.6	9390	774	53	1.23	1.73	42.7	20
11	50.2	9625	775	58	1.21	1.64	37.6	17
12	50.9	9755	761	47	1.20	1.63	37.2	17
13	49.8	10245	760	53	1.13	1.50	29.0	14
14	49.6	9690	769	41	1.20	1.63	36.4	17
15	50.3	9205	753	56	1.27	1.83	48.4	22
16	50.0	9705	74[illegible]	58	1.20	1.62	36.6	17

[a]Measured at room temperature; includes fuel pin simulator (FPS), pressure transducer, and connecting tube.

[b]Ratio of initial pressure to burst pressure.

[c]Ratio of final to initial gas volume; includes FPS, pressure transducer, and connecting tube.

[d]Obtained from deformation profiles assuming circular cross sections.

[e]Assumes volume increase is uniformly distributed over heated length.

[f]Simulator developed leak during transient; deformation behavior is abnormal.

[g]Simulator developed leak prior to test; attempts to compensate for leak resulted in tube being tested at essentially constant pressure.

calculated the percentage of coolant-channel flow area restriction with the rod-centered unit cell method, using the equation

$$B = 100 \times \frac{\sum^{n=16} (A_{d,n} - A_o)}{16(p^2 - A_o)},$$

where

B = percentage restriction in coolant-channel flow area,
$A_{d,n}$ = outside area of deformed tube (mm^2),
A_o = outside area of original tube (mm^2),
p = tube-to-tube pitch in square array (mm).

With this definition, B is zero for no deformation and 100 if all the tubes deform into a square whose sides are of length p (completely filling the open area). For the case of uniform ballooning such that the tubes just come into contact (32% strain for the dimensions appropriate to this test), B is 61%.

In summing the deformed tube areas in the above equation for those sections that contain bursts, one must decide how to treat the burst tube flare-out. We used two definitions that appear to be reasonable upper and lower limits of the coolant-channel flow area restriction. The first definition, which we believe is representative of the upper limit, consists of drawing straight lines between the ends of the tube flare-outs to establish a burst tube area, as illustrated in Fig. 2.24. Special consideration was given to those flare-outs that enclosed adjacent tubes to exclude overlapping areas, as noted by tube 4 in the figure. The second definition, which we believe is representative of the lower limit, considered the burst tube cross section as a circle with a perimeter equal to that of the tube, as illustrated by tube 7 in the figure. The latter definition is considered a reasonable approximation of the tube just before burst.

The deformed tube areas were obtained by the data analysis techniques reported[3] for the B-1 test. Table 2.5 gives the deformed tube areas, $A_{d,n}$, for each tube at each section based on the first definition for the burst tube area, and Table 2.6 gives similar information based on

Table 2.5. Upper limit of B-3 deformed tube areas (mm^2)

ELEVATION (cm)	TUBE NO. 1	2	3	4	5	6	7	8	9	10	11	12	13	14	15	16	TOTAL
0.0	94	94	94	94	94	94	93	93	94	93	93	93	94	94	94	94	1504
1.8	98	96	100	97	96	97	96	95	96	97	98	100	102	98	95	96	1563
3.5	105	108	113	107	103	110	110	107	106	115	107	107	105	107	106	104	1727
5.0	107	121	118	112	106	116	118	116	112	124	111	108	104	111	121	109	1820
6.7	105	120	110	110	106	112	116	113	111	118	110	105	103	109	120	107	1781
8.7	98	106	100	102	100	102	102	101	100	103	100	98	98	99	104	98	1615
11.6	103	105	104	103	103	105	107	103	102	107	104	103	106	103	104	102	1671
13.4	119	121	116	118	115	122	129	120	115	129	122	121	130	119	125	119	1947
15.3	126	141	126	138	131	141	138	131	127	148	127	131	154	132	172	136	2208
17.2	126	141	133	152	143	145	142	132	133	150	142	130	132	126	208	155	2307
19.0	131	150	135	198	141	152	147	142	145	157	166	129	120	150	220	159	2492
20.7	128	162	131	292	140	164	154	148	155	175	168	132	115	147	230	164	2611
22.5	132	160	130	182	154	174	161	150	156	249	167	143	116	144	214	168	2610
24.2	135	170	140	147	179	176	169	153	165	270	188	161	122	157	191	172	2319
25.6	136	186	153	176	263	179	183	158	209	205	242	167	133	187	169	195	2365
26.8	136	194	161	184	421	206	175	150	217	182	204	160	144	291	157	143	3147
28.2	139	184	159	191	325	239	158	143	200	167	158	154	164	167	145	152	2943
29.7	137	175	152	162	181	203	149	142	176	149	142	152	279	151	157	152	2466
31.3	129	181	146	145	153	154	148	144	165	142	137	155	187	144	191	145	2474
32.6	124	195	144	139	145	143	158	148	156	140	136	156	149	139	247	137	2464
33.8	118	196	143	140	137	141	161	145	145	137	135	153	133	131	315	137	2676
35.0	120	198	158	148	140	147	167	145	142	137	134	145	130	130	204	140	2361
36.1	120	195	209	154	140	146	167	148	136	133	134	137	131	130	171	145	2403
37.5	121	221	330	160	139	145	168	142	131	132	136	137	142	132	164	148	2577
39.2	132	417	197	160	135	145	181	185	137	138	134	140	166	140	164	144	2729
40.8	147	263	153	160	145	155	192	201	162	155	137	145	162	147	157	143	2630
42.4	146	196	157	160	154	157	185	225	194	156	135	155	138	148	151	146	2408
44.0	144	185	170	165	156	155	192	344	236	148	134	163	130	153	154	144	2781
45.2	152	188	169	170	162	158	277	340	279	150	137	171	129	153	156	137	2976
46.8	158	194	173	172	177	176	330	233	210	157	141	199	129	147	154	133	2360
48.3	153	172	182	179	182	179	206	176	181	161	136	343	123	136	143	114	2762
50.0	176	164	214	167	176	174	170	158	175	166	137	175	124	138	137	135	2594
51.6	280	168	180	146	152	166	163	151	164	166	136	148	121	137	137	131	2554
52.9	200	171	153	138	144	160	155	142	159	160	133	135	122	136	139	129	2383
54.3	152	154	136	137	138	150	144	137	147	147	131	130	116	130	136	125	2218
55.8	134	141	129	133	137	140	137	140	138	139	129	126	116	128	131	124	2125
57.5	130	134	126	131	132	128	135	143	131	130	127	122	115	128	124	120	2042
59.2	129	129	121	133	124	124	133	135	124	126	124	118	114	126	121	115	2002
61.0	120	117	114	120	114	116	118	118	114	117	114	111	110	116	114	110	1960
62.9	102	102	101	101	102	102	102	100	100	102	100	99	100	101	101	99	1622
65.8	104	104	102	101	102	103	103	103	103	101	102	99	99	101	101	99	1628
67.8	123	116	115	115	113	117	114	116	111	110	115	108	103	110	108	108	1808
69.5	148	126	125	129	124	129	120	127	120	119	123	118	108	122	114	110	1980
71.2	157	131	128	134	124	127	119	129	119	115	123	114	104	124	111	117	1985
72.9	164	139	128	143	125	129	122	131	124	118	128	115	105	130	115	119	2038
74.6	159	140	126	161	126	128	124	129	125	120	127	119	109	132	117	120	2368
76.4	145	133	122	174	120	126	120	126	119	115	124	121	108	128	114	117	2319
78.2	141	133	122	170	118	127	121	131	121	115	125	122	110	129	113	117	2022
80.1	135	131	121	154	116	130	119	124	121	114	124	117	109	129	114	113	1979
82.0	127	128	117	135	115	128	115	114	116	111	118	114	107	120	114	111	1897
83.8	119	124	111	116	113	117	110	109	115	110	113	112	107	114	113	111	1820
85.6	114	115	106	108	109	108	105	105	111	106	107	106	105	106	107	106	1729
87.5	106	102	100	102	100	101	100	100	101	100	101	97	99	100	102	103	1627
89.5	98	96	96	98	95	96	95	95	94	94	95	94	94	94	96	95	1530
91.5	96	95	95	96	94	95	94	95	95	95	94	94	94	94	95	93	1520

Table 2.6. Lower limit of B-3 deformed tube areas (mm^2)

ELEVATION (cm)	TUBE NO.																
	1	2	3	4	5	6	7	8	9	10	11	12	13	14	15	16	TOTAL
0.0	94	94	94	94	94	94	93	93	94	93	93	93	94	94	94	94	1504
1.8	98	96	100	97	96	97	96	95	96	97	98	100	102	98	95	96	1563
3.5	105	108	113	107	103	110	110	107	106	115	107	107	105	107	106	104	1727
5.0	107	121	118	112	106	116	118	116	112	124	111	108	104	111	121	109	1820
6.7	105	120	110	110	106	112	116	113	111	118	110	105	103	109	120	107	1781
8.7	98	106	100	102	100	102	102	101	100	103	100	98	98	99	104	98	1615
11.6	103	105	104	103	103	105	107	103	102	107	104	103	104	103	104	102	1671
13.4	119	121	116	118	115	122	129	120	115	129	122	121	130	119	125	119	1947
15.3	126	141	126	138	131	141	138	131	127	146	127	131	154	132	172	139	2208
17.2	126	141	133	152	143	145	142	132	133	150	142	130	132	136	208	155	2307
19.0	131	150	135	198	141	152	147	142	145	157	166	129	120	150	220	159	2452
20.7	128	162	131	240	140	164	154	148	155	175	168	132	115	147	230	164	2566
22.5	132	160	130	182	154	174	161	150	156	210	167	143	116	144	214	198	2601
24.2	135	170	140	167	179	174	169	153	165	219	188	161	122	157	191	232	2727
25.6	136	186	153	176	216	179	183	158	209	205	235	167	133	187	169	195	2965
26.8	136	194	161	194	254	206	175	150	217	182	204	160	144	184	152	143	2873
28.2	139	164	159	181	196	236	158	143	200	167	158	154	168	167	145	152	2712
29.7	137	175	152	162	181	203	149	142	176	149	142	152	219	151	157	152	2605
31.3	129	181	146	145	153	154	148	144	165	142	137	155	187	144	191	145	2474
32.6	124	195	144	139	145	143	158	148	156	140	136	156	149	139	247	137	2464
33.9	118	196	143	140	137	141	161	145	145	137	135	153	133	131	228	137	2388
35.0	120	198	158	148	140	147	167	145	142	137	134	145	130	130	204	140	2391
36.1	120	195	209	154	140	146	167	148	136	133	134	137	131	130	171	145	2403
37.5	121	221	283	160	139	145	168	142	131	132	134	137	142	132	164	148	2529
39.2	132	289	197	160	135	145	181	185	137	138	134	140	166	140	164	144	2567
40.8	147	263	153	160	145	155	192	201	162	155	137	145	142	147	157	143	2430
42.4	146	196	157	160	154	157	185	225	194	156	135	155	136	148	151	146	2406
44.0	144	185	173	165	156	155	192	287	236	149	134	163	130	153	154	144	2773
45.2	152	188	169	170	162	158	203	294	236	150	137	171	129	153	156	137	2771
46.8	158	194	173	172	177	176	244	233	210	157	141	199	129	147	154	133	2804
48.3	153	172	182	179	182	175	206	176	181	161	136	207	123	136	143	134	2652
50.0	176	164	214	167	176	174	170	158	175	166	137	175	124	138	157	135	2604
51.6	205	168	180	146	152	166	163	151	164	166	136	148	121	137	137	131	2479
52.5	200	171	153	138	144	160	155	142	155	160	133	135	122	136	139	129	2383
54.3	152	154	136	137	138	150	144	137	147	147	131	130	116	130	136	125	2218
55.8	134	141	129	133	137	140	137	140	138	139	129	126	114	128	131	124	2129
57.5	130	134	126	131	132	128	135	143	131	130	127	122	115	128	124	120	2049
59.2	129	129	121	133	124	124	133	135	124	126	124	118	114	126	121	115	2002
61.0	120	117	114	120	114	116	118	118	114	117	114	111	110	116	114	110	1850
62.9	102	102	101	101	102	102	102	100	100	102	100	99	100	101	101	99	1623
65.8	104	104	102	101	102	103	103	103	103	101	102	99	99	101	101	99	1634
67.8	123	116	115	115	113	117	114	116	111	110	115	108	103	110	108	108	1908
69.5	148	126	125	129	124	125	120	127	120	119	123	118	108	122	114	119	1990
71.2	157	131	128	134	124	127	119	129	119	115	123	114	104	124	111	117	1985
72.9	164	139	128	143	125	129	122	131	124	118	128	115	105	130	115	119	2039
74.6	158	140	126	161	126	128	124	129	125	120	127	119	109	132	117	120	2049
76.4	145	133	122	174	120	126	120	126	119	115	124	121	108	128	114	117	2019
78.2	141	133	122	170	118	127	121	131	121	115	125	122	110	129	113	117	2027
80.1	135	131	121	154	116	130	119	124	121	114	124	117	109	129	114	113	1979
82.0	127	128	117	135	115	128	115	114	116	111	118	114	107	120	114	111	1897
83.8	119	124	111	116	113	117	110	109	115	110	113	112	107	114	113	111	1920
85.6	114	115	106	108	109	108	105	105	111	106	107	106	105	106	107	106	1729
87.5	106	102	100	102	100	101	100	100	101	100	101	97	99	100	102	103	1622
89.5	98	96	96	98	95	96	95	95	94	94	95	94	94	94	96	95	1530
91.5	96	95	95	95	94	95	94	95	95	95	94	94	94	95	95	93	1520

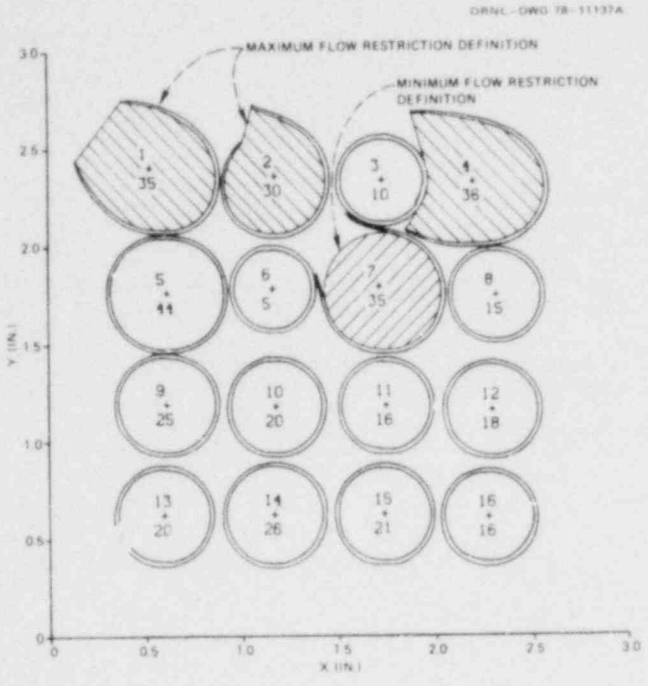

Fig. 2.24. An example of a computer simulation of a bundle cross section showing the definitions for maximum and minimum flow restrictions for burst tubes.

the second definition. The last column (on the right side) gives the summation of the individual $A_{d,n}$. The summed areas were used in the above equation to calculate the coolant-channel flow area restriction at each section; the results are given in Table 2.7 and plotted in Fig. 2.25 as a function of heated length. The flow channel restriction differs only in the sections where tube bursts occurred. The cross-sectional area occupied by the grids (about 47 mm^2) was not included in the calculation; including this area would slightly increase the restriction at the grid locations (centered about elevations 10 and 66 cm). The maximum restriction (at elevation 26.8 cm) was 90 or 75%, depending on which method for handling the tube flare-out was used.

It will be noted that the two maxima in the figure (at the 26.8- and 45.2-cm elevations) correspond to the regions of strains greater than 32% in the individual tubes (see Fig. 2.22).

Since the major difference between the B-3 and B-1 tests was the heating rate (9.5°C/sec for B-3 vs 30°C/sec for B-1), it is of interest to compare the coolant flow area reduction for the two tests. Figure 2.26

Table 2.7. B-3 coolant channel restriction

Elevation (cm)	Upper limit (%)	Lower limit (%)
0.0	0.4	0.4
1.8	3.5	3.5
3.5	12.5	12.5
5.0	17.6	17.6
6.7	15.4	15.4
8.7	6.3	6.3
11.6	9.4	9.4
13.4	24.5	24.5
15.3	38.7	38.7
17.2	44.2	44.2
19.0	52.0	52.0
20.7	60.7	57.9
22.5	62.3	60.2
24.2	77.6	67.1
25.6	79.2	76.3
26.8	90.0	75.1
28.2	73.4	66.2
29.7	63.7	60.4
31.3	53.3	53.3
32.6	52.7	52.7
33.8	53.4	48.6
35.0	48.8	48.8
36.1	49.4	49.4
37.5	58.9	56.3
39.2	67.0	60.0
40.8	61.8	61.8
42.4	60.6	60.6
44.0	70.0	66.9
45.2	78.5	69.5
46.8	76.0	71.3
48.3	70.7	63.0
50.0	59.8	59.8
51.6	57.6	53.5
52.9	48.3	48.3
54.3	39.3	39.3
55.8	34.4	34.4
57.5	30.8	30.8
59.2	27.5	27.5
61.0	19.2	19.2
62.9	6.7	6.7
65.8	7.4	7.4
67.8	16.9	16.9
69.5	26.3	26.3
71.2	26.5	26.5
72.9	29.5	29.5
74.6	31.1	31.1
76.4	28.4	28.4
78.2	28.6	28.6
80.1	26.3	26.3
82.0	21.8	21.8
83.8	17.6	17.6
85.6	12.6	12.6
87.5	6.7	6.7
89.5	1.7	1.7
91.5	1.2	1.2

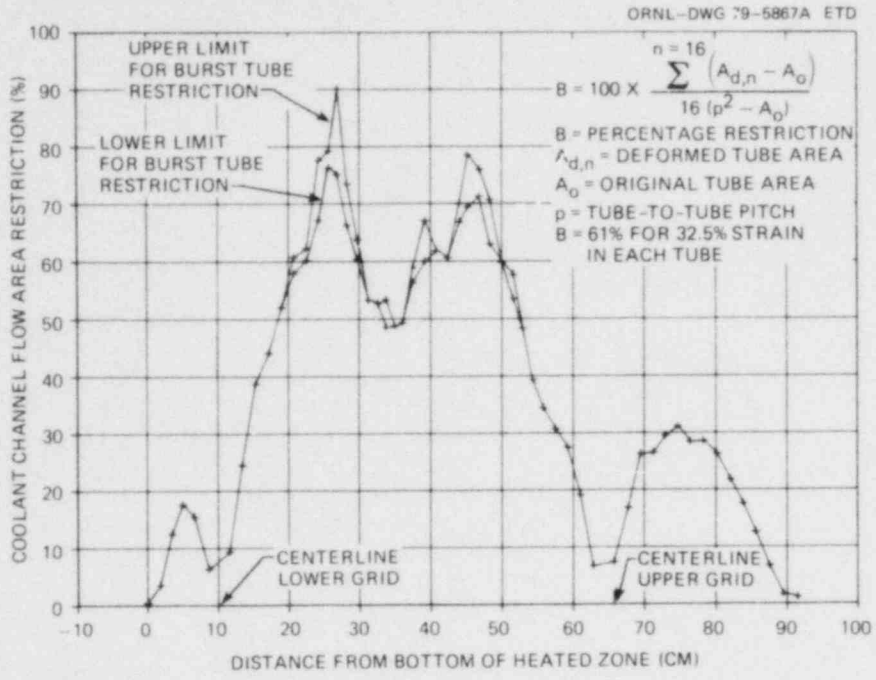

Fig. 2.25. Coolant-channel flow area restriction in B-3 based on rod-centered unit cell and estimated upper and lower limits of burst tube flow restriction.

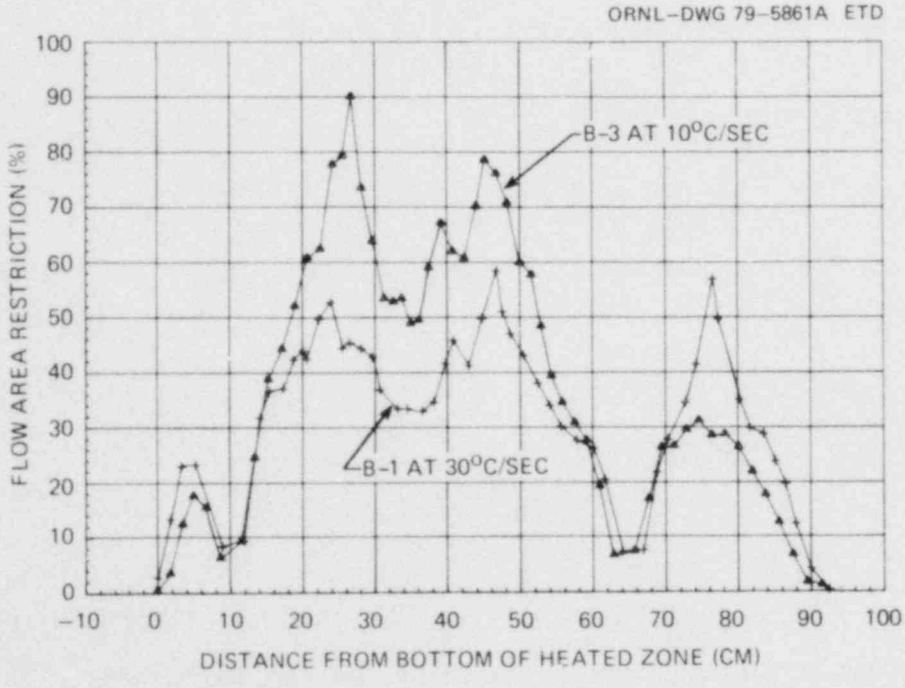

Fig. 2.26. Comparison of B-3 and B-1 coolant-channel restriction based on maximum flow retriction definition.

makes this comparison on the basis of the maximum flow restriction definition, and Fig. 2.27 shows the comparison based on the minimum flow restriction definition. The figures show great similarity, as expected, since the same fuel simulators were used in the two tests. Due to the interdependent relationship between steam flow rate and bundle heating rate, the upper 25 cm of the heated zone was relatively cooler in the B-3 test, and less deformation occurred in this region than in the B-1 test.

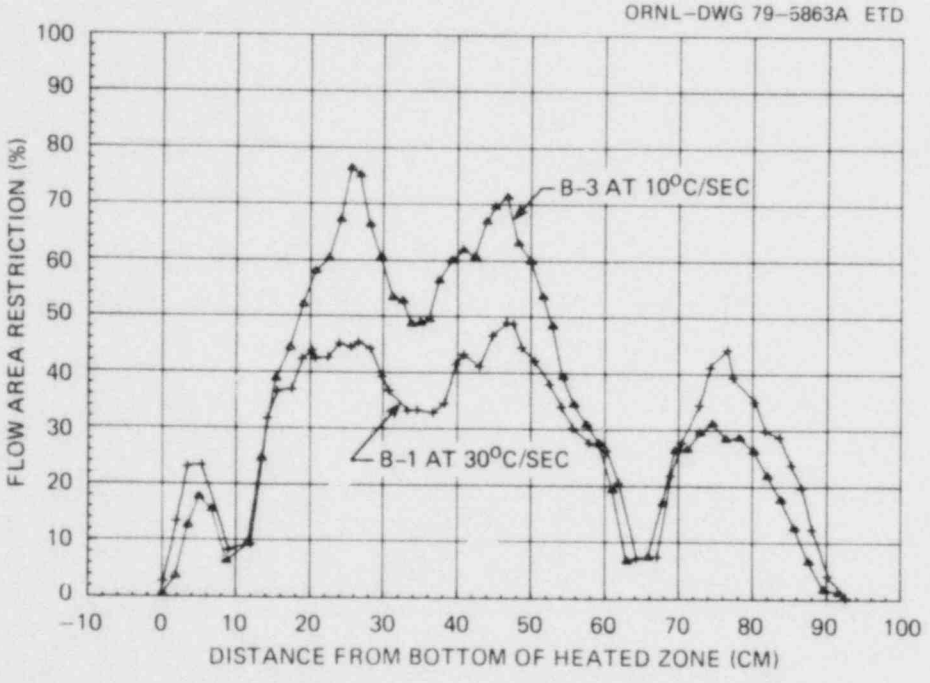

Fig. 2.27. Comparison of B-3 and B-1 coolant channel restriction based on minimum flow restriction definition.

2.4 Digital Simulation of Bundle Tests

M. D. White L. J. Ott
R. D. Dabbs

Work has been under way to develop a transient digital simulator of the MRBT facility to facilitate establishment of inlet steam conditions for future bundle tests. Preliminary investigation of experimental data has shown that both steam flow rate and bundle heating rate have an effect

on the axial location of simulator bursts. In addition, the axial temperature profiles indicate that both radiation and convection heat transfer may be important.

Effort this reporting period was concentrated on development of a thermal-hydraulics computer program to model fuel-pin simulators and channels. A model of a corner fuel-pin simulator and flow channel was developed which closely approximated the observed behavior in the B-2 test. Using the code, it was possible to approach the time-temperature history of this part of test, with calculated burst temperature ranges being achieved at approximately the observed burst times. Currently, work is under way to model other channels (wall and interior) and other tests (B-1 and B-3). This modeling is necesary to verify the code's predictive capabilities under a variety of situations. Verification of the predictive capabilities is important because the code requires detailed knowledge of inlet and outlet boundary conditions, which must be estimated for future tests on the basis of past performance. Once suitable verification of these tests is achieved, the code will be ready to use as a predictive tool in establishing test conditions for future tests.

3. DEVELOPMENT AND PROCUREMENT

3.1 Temperature Control Systems

K. R. Carr*

A dolly-mounted 375-kW solid-state power supply has been procured to supply dc power for independent heating of the shroud (when desired) in either the multirod or the single-rod test facility. This power supply and the one connected to the bundle or the single-fuel-pin simulator (as the case may be) are controlled by an integrated system of controllers which automatically controls the shroud and test assembly temperatures in accordance with preprogrammed temperature paths that may involve temperature ramps, constant temperature, and/or combinations of the two. A unique feature of the control system is the ability to electronically average signals of up to eight thermocouples on both the shroud and the test assembly for use in the feedback control loop. The circuitry automatically excludes from the averaging process any signal that deviates from the average or the set point by a preprogrammed amount. The design of the system was described in the previous report.[10]

During this reporting period, checkout and demonstration of proper control action over a wide range of test conditions were completed in a series of equipment development tests involving both the multirod and the single-rod test facilities. Based on experience gained in these tests, it was decided to limit control action on the test assembly to proportional control and on the shroud to a combination of proportional and integral control. It was necessary to remove the output signal clamping diodes, since they interfered with proper temperature control action in some cases. Other protective features, such as automatic exclusion of out-of-limits control thermocouples, are adequate to provide the protection for which the diodes were intended.

Some response features of the control system are illustrated in Fig. 3.1, which is a quick-look plot of data taken during a bundle-with-heated-shroud development test (No. B4ST-5B). The 4 × 4 bundle was

---

*Instrumentation and Controls Division.

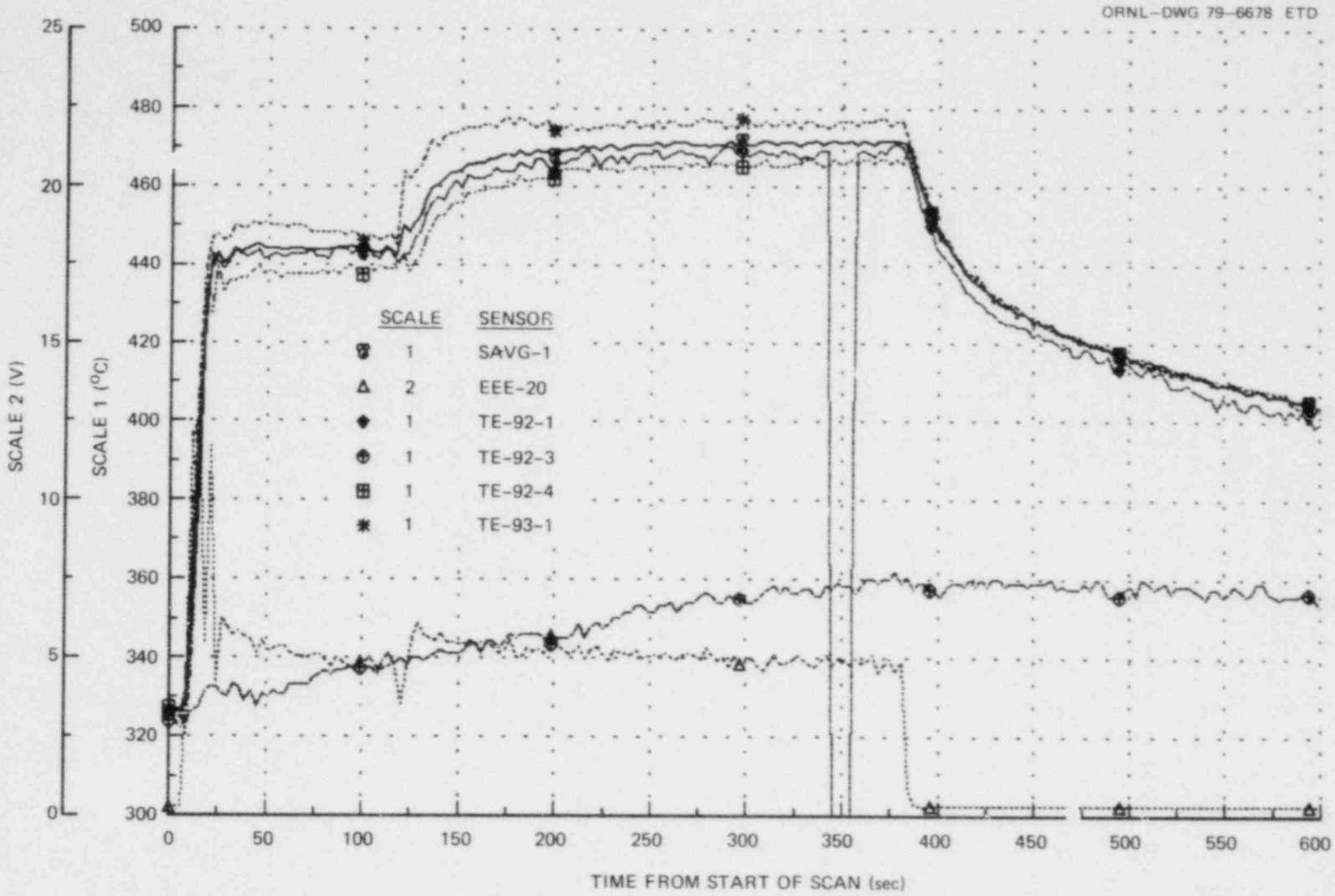

Fig. 3.1. Example of temperature control system stability when one or more control thermocouples are lost. TE 92-3 was lost during the ramp (at about 20 sec). TE 92-1 was unplugged and replugged at about 342 and 353 sec respectively.

simulated by the use of four fuel-pin simulators, which were unpressurized to prevent deformation during the test. In this plot, the "SAVG-1" trace is the average of those shroud control thermocouples which are within the set-point limits (±75°C), the "EEE-20" trace is the shroud applied voltage, and the remaining traces (TE 92-1, TE 92-3, TE 92-4, and TE 93-1) are temperatures indicated by shroud control thermocouples.

The main features illustrated in the figure include the automatically controlled initial temperature ramp to about 440°C, a period (about 100 sec) of constant temperature, a 30°C manual change in temperature set point at about 125 sec, followed by a period (about 250 sec) of constant temperature. Control system response to both a real and a simulated loss of a control thermocouple is also evident in the figure. The real loss occurred during the initial temperature ramp by failure of TE 92-3, and the simulated loss was produced by disconnecting TE 92-1 at about 342 sec and reconnecting it at about 352 sec. The latter event, shown on an expanded time and temperature scale in Fig. 3.2, was designed to simulate a control thermocouple first becoming open-circuited and then close-circuited. Neither the real nor the simulated loss of control thermocouples caused a discernible change in shroud applied voltage or indicated shroud average temperature. The responses show that the control system is able to continue an experiment under controlled temperature conditions without significant perturbations in the event that one or more of the control thermocouples fail.

3.2 4 × 4 Bundle Shroud Heating Tests

J. L. Crowley K. R. Carr*
A. W. Longest

In some 4 × 4 bundle tests, it is desired to have the average temperature of the shroud surrounding the bundle test array closely follow the average temperature of the bundle. This was attempted in the B-1 and B-3 tests by electrically connecting the shroud in series with the bundle

*Instrumentation and Controls Division.

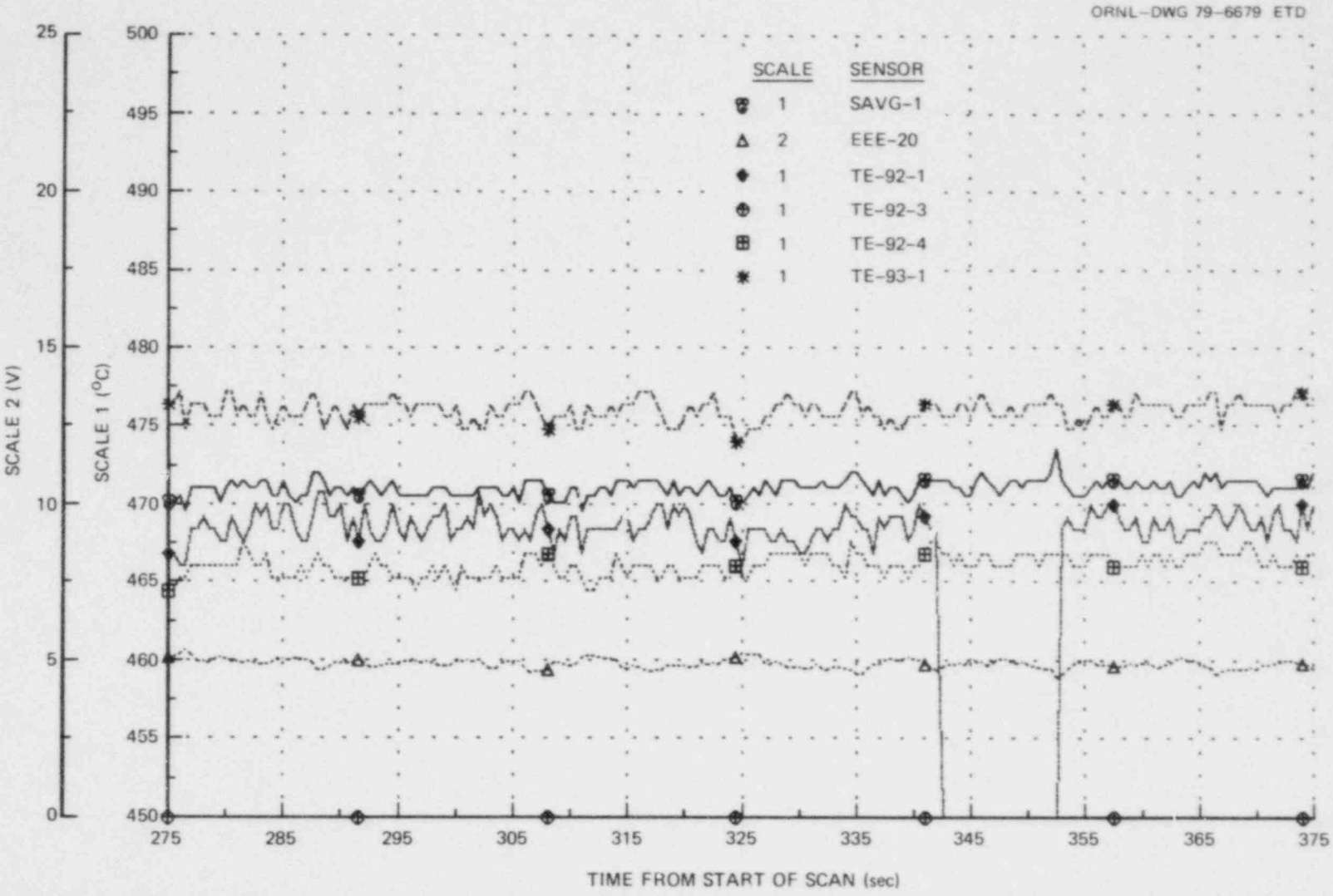

Fig. 3.2. Expanded time scale portion of test B4ST-5B showing control system stability during unplugging and replugging TE 92-1 at about 342 and 353 sec respectively.

in order that a single power supply could be used for both purposes. This arrangement was not totally satisfactory in that the shroud temperature lagged the bundle temperature by an increasing amount as the transient progressed. This situation results from the inability to match shroud and bundle electrical and heat loss characteristics throughout the transient; the predominant c use appears to be an increasing portion of the shroud input power being dissipated by heat losses as the temperature increases, while the losses from the bundle remain a relatively small fraction of its input power. A separate dc power supply for heating the shroud has been incorporated in the test facility to improve the temperature match between the shroud and bundle throughout the transient. The power supply, capable of supplying up to 2500 A at 150 V, and its associated control equipment are portable and will be used in both the multirod and the single-rod test facilities. Design of the complex control system was described in the previous report;[10] checkout and performance verification of the design features were discussed in the preceding section.

Operation of the integrated system was demonstrated with a shroud heating test assembly in a series of tests designated with the prefi:. B4ST. The test assembly, which incorporated four unpressurized fuel-pin simulators to model a 4 × 4 bundle, was subjected to numerous temperature ramps and maintained at an elevated temperature (about 750°C) for relatively long periods of time in both air and steam environments to determine operating procedures, controller settings, power supply characteristics, etc., necessary to integrate operation of the various subsystems. A series of 18 tests, involving approximately 50 temperature ramps, were conducted in an iterative manner over a period of about two months to perfect integration of the subsystems. The tests involved temperature ramp rates of 10 and 30°C/sec and constant-temperature hold times of 1[illegible] to 400 sec at temperatures up to 750°C. The steam flow rate was varie[illegible] from about 2.3 to about 5.6 kg/hr, covering the range used in previous single-rod and bundle tests.

The final test, identified as BS4T-5D, may be used as an illustrative example of the performance of the integrated system in the multirod test facility. This particular test incorporated a 10°C/sec ramp to

760°C followed by a period (about 200 sec) of constant temperature to simulate an isothermal creep-rupture test. Figure 3.3 is a quick-look data plot of a major portion of the test, showing bundle and shroud average temperatures (KAVG-1 and SAVG-1 respectively) and the applied bundle and shroud voltages (EEE-10 and EEE-20 respectively). The downward spike in SAVG-1 at about 27 sec is due to a momentary data-processing problem in the computer-controlled data acquisition system. As is evident, the shroud temperature closely followed the bundle temperature during the constant-temperature portion of the test and was in acceptable agreement during the initial ramp. Note the relatively small difference in shroud voltage during the ramp and constant-temperature portions of the test, whereas the voltage required to maintain the bundle at constant temperature was drastically reduced from that required for the ramp.

Figure 3.4 shows the steam inlet (TE 310) and outlet (TE 305) temperatures in relation to the bundle average (KAVG-1) and shroud average (SAVG-1) temperatures. The steam flow rate for this test was about 2.5 kg/hr, which for the 4-rod test array corresponds to a Reynolds number equal to that for the 16-rod B-3 test with a flow rate of 4.5 kg/hr. The ratio of steam mass flow rate to heated surface area was also the same in the two tests due to the equivalent hydraulic diameter relationship. The steam outlet temperature appears to be more closely coupled to the shroud temperature than to the 4-rod bundle.

3.3 Single-Rod Shroud Heating Tests

J. L. Crowley
K. R. Carr*
A. W. Longest
D. B. Lloyd

Preparation of the single-rod test facility for the start of a new series of single-rod tests incorporating a heated shroud was completed during this report period. This important development activity included the facility modifications described in Sect. 4.5 and the shakedown and demonstration tests of the new systems described below. The heated-shroud assembly will permit single-rod testing under thermal conditions closely

*Instrumentation and Controls Division.

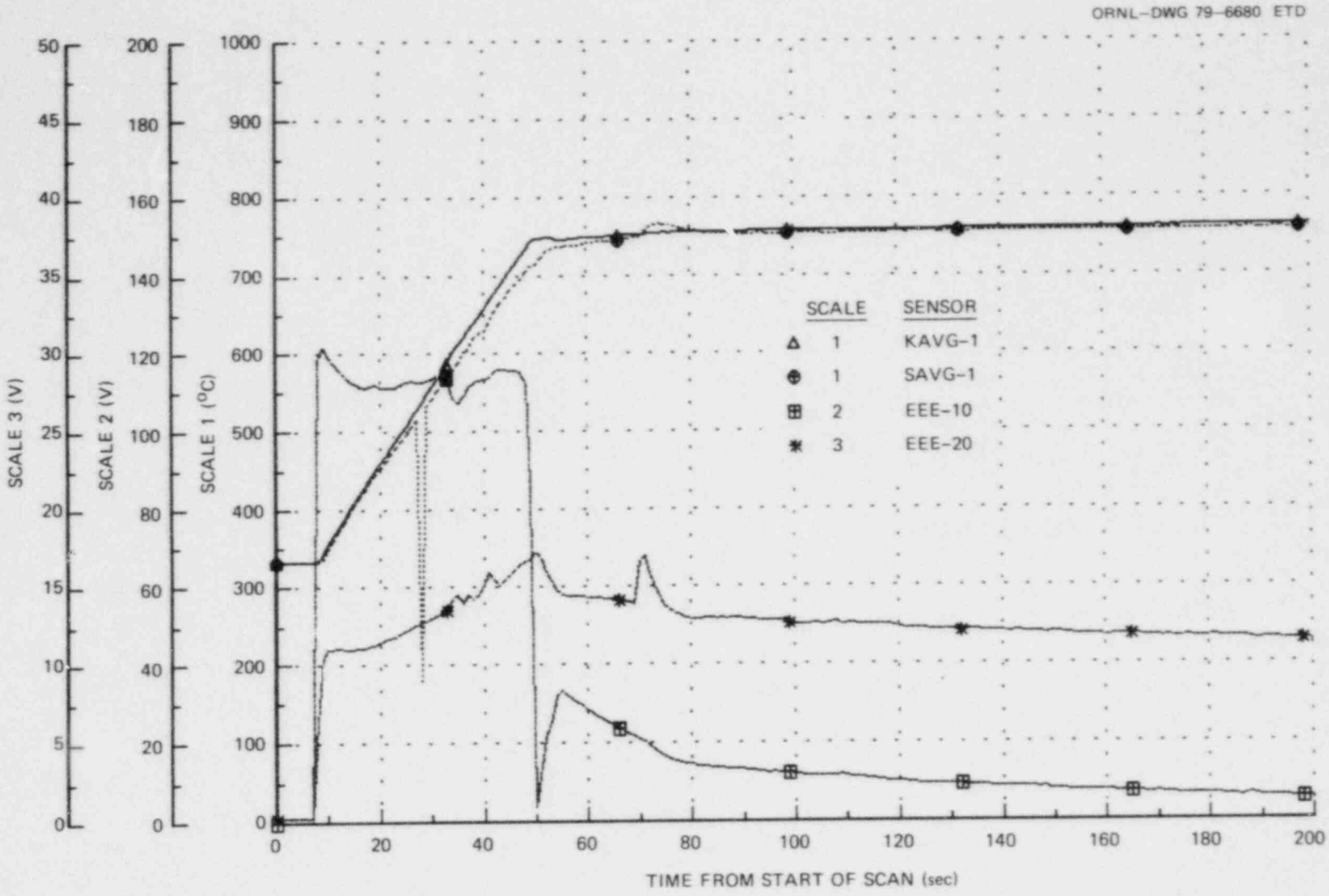

Fig. 3.3. Shakedown test No. B4ST-5P showing average temperatures of four FPS (KAVG-1) and of shroud (SAVG-1). The power required is represented by the FPS voltage (EEE-10) and shroud voltage (EEE-20).

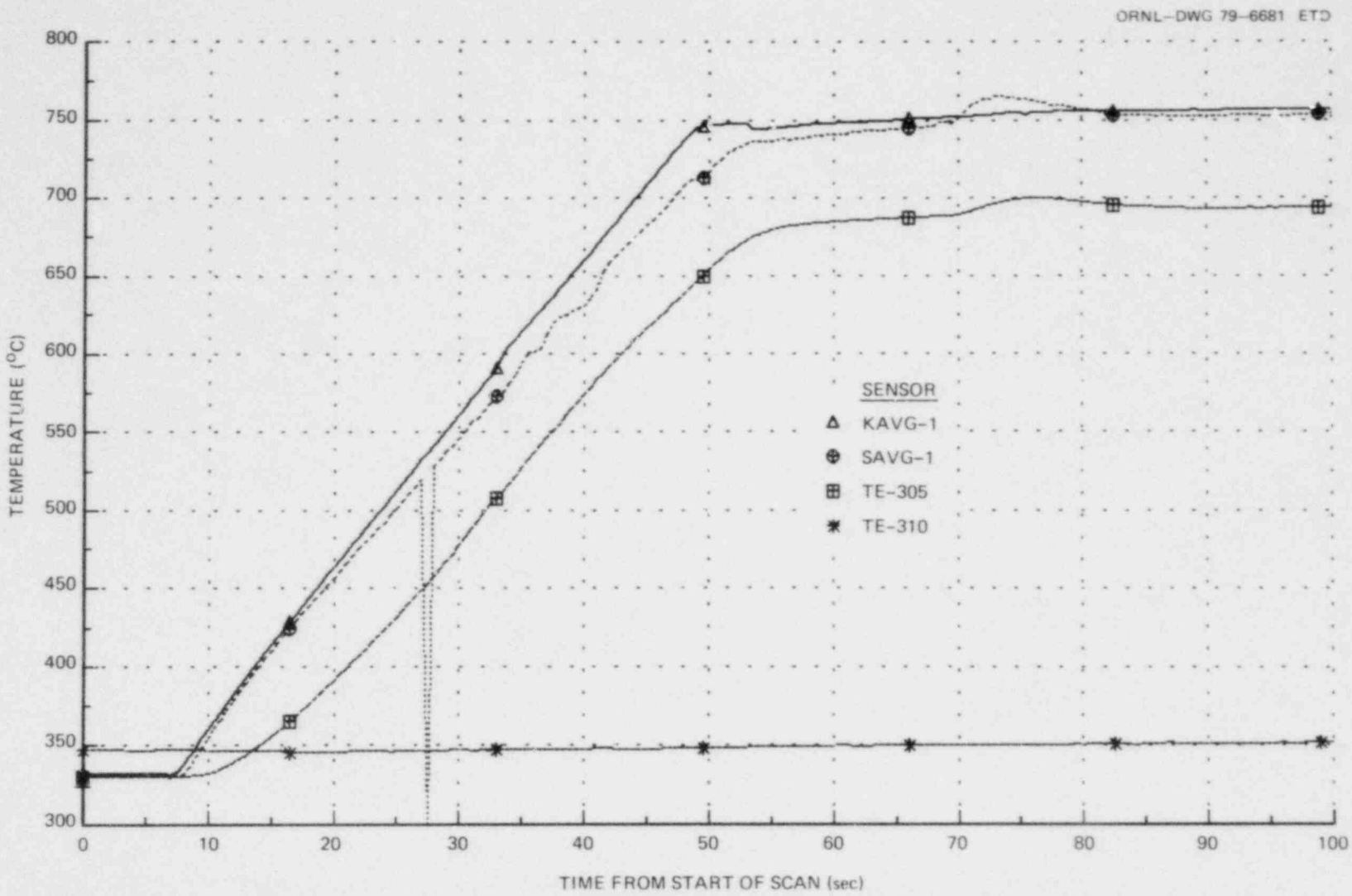

Fig. 3.4. Shakedown test No. B4ST-5D showing average temperatures of four FPS (KAVG-1) and of shroud (SAVG-1) and bundle steam inlet (TE 310) and outlet (TE 305) temperatures.

matching conditions in a bundle, and tube deformation behavior should be close to that in a bundle except for the influences of rod-to-rod interactions and radial restraint.

New systems requiring shakedown, in addition to the new test assembly, included the shroud portable power supply and the temperature control systems previously used only in the B4ST demonstration tests in the multirod test facility (see Sect. 3.2). The new temperature control systems, described in detail in the previous progress report[10] and in Sect. 3.1 of this report, are designed to automatically control the shroud and fuel-pin simulator (FPS) temperatures along a preprogrammed path and thereby provide needed improvement in temperature control in both the single-rod and bundle tests. The experience gained in operation of the power supplies and temperature controllers in the multirod facility demonstration tests expedited setup and checkout of the new systems at the single-rod facility.

Fuel-pin simulator SR-30 was used in the heated-shroud single-rod shakedown and demonstration tests. Twelve bare-wire (0.25-mm-diam) type S thermocouples were spot-welded to the outside of the Zircaloy tube to provide cladding temperature measurements. Four thermocouples, equally spaced around the tube, were located at each of three axial locations selected on the basis of the pretest infrared characterization scan of the fuel simulator (internal heater). Eight of the thermocouples were connected to the FPS temperature controller for generation of the average temperature signal used as the FPS temperature feedback control signal.

Six bare-wire (0.25-mm-diam) type S thermocouples were spot-welded directly to the shroud, with two each, 180° apart, at each of three axial locations to provide shroud temperature data. All six thermocouples were connected to the shroud temperature controller for generation of the average temperature signal used as the shroud temperature feedback control signal.

Test conditions for the SR-30 shakedown and demonstration tests are summarized in Table 3.1. The initial conditions were typical of those employed in most of the previous single-rod tests. However, the initial pressure was set low to preclude tube deformation except in the last test

Table 3.1. Summary of test conditions for the SR-30 series of demonstration tests

Test No.	Initial conditions				Cladding heat rate (°C/sec)	Power to shroud	Temperature for power off, change of heat rate, or hold point (°C)	Hold time (sec)
	Temperature (°C)	Differential pressure (kPa)	Steam flow rate (kg/hr)	Inlet Reynolds No.				
SR-30 A	340	690	2.09	740	10	No	450	100
SR-30 B	340	690	2.09	740	10	No	760	100
SR-30 C	340	690	2.09	740	10	Yes	450	200
SR-30 D	340	690	2.09	740	10	Yes	760	100
SR-30 E	340	690	2.09	740	10	Yes	860	0
SR-30 F	340	690	2.09	740	28	Yes	450	0
SR-30 G	340	6480[a]	2.09	740	28	Yes	860	0
SR-30 H	340	690	2.09	740	5	Yes	860	0
SR-30 I	340	690	2.09	740	10[b]	Yes	700	0
					2[b]	Yes	860	0
SR-30 J	340	690	2.09	740	28	Yes	600	100

[a] Test SR-30 G was the last test performed, and the initial pressure was set to cause tube burst at about 860°C.

[b] Test SR-30 I included an initial heating rate of 10°C/sec, and when the temperature reached 700°C the heating rate was decreased to 2°C/sec.

performed, SR-30 G, in which the tube was pressurized to permit observation of the system responses to tube deformation and burst.

The SR-30 test series was carried out successfully, and, in general, the results indicated good performance of the new test assembly and temperature control systems. Quick-look data plots showing some of the performance capability and characteristics of the new facility are given in Figs. 3.5 (SR-30 D test) and 3.6 (SR-30 I test). In these figures, SAVG-1 is the average temperature generated from the signals of the six shroud thermocouples, RAVG-1 is the average temperature generated from the signals of the eight FPS thermocouples connected to the FPS temperature controller, EIM-9 is the FPS current, and EIM-300 is the shroud current. As can be seen in the figures, a slight mismatch of the shroud and FPS average temperatures occurred during changeover from one heating rate to another, but the mismatch was small in magnitude and of sufficiently short duration to be of only minor concern.

In carrying out the SR-30 tests, controller system settings were recorded for future reference, and the operating procedures were verified and corrected as needed. These records, together with the data collected on the CCDAS, provide sufficient information to permit future tests to be set up under a wide range of test conditions without the need of further practice runs.

Although the SR-30 G test was terminated by the tube bursting as planned, the test is regarded as "sacrificial" because of its complex thermal history and repeated subjection to steam oxidation. We do not plan further evaluation or reporting of results from the SR-30 G burst test, since they appear to be of little value to the program.

3.4 Thermocouple Development and Procurement

K. R. Carr* J. H. Holladay*

Delivery on an order for 300 Inconel-sheathed (0.71-mm-OD) type K thermocouples for the B-5 fuel-pin simulators, originally scheduled for

---

*Instrumentation and Controls Division.

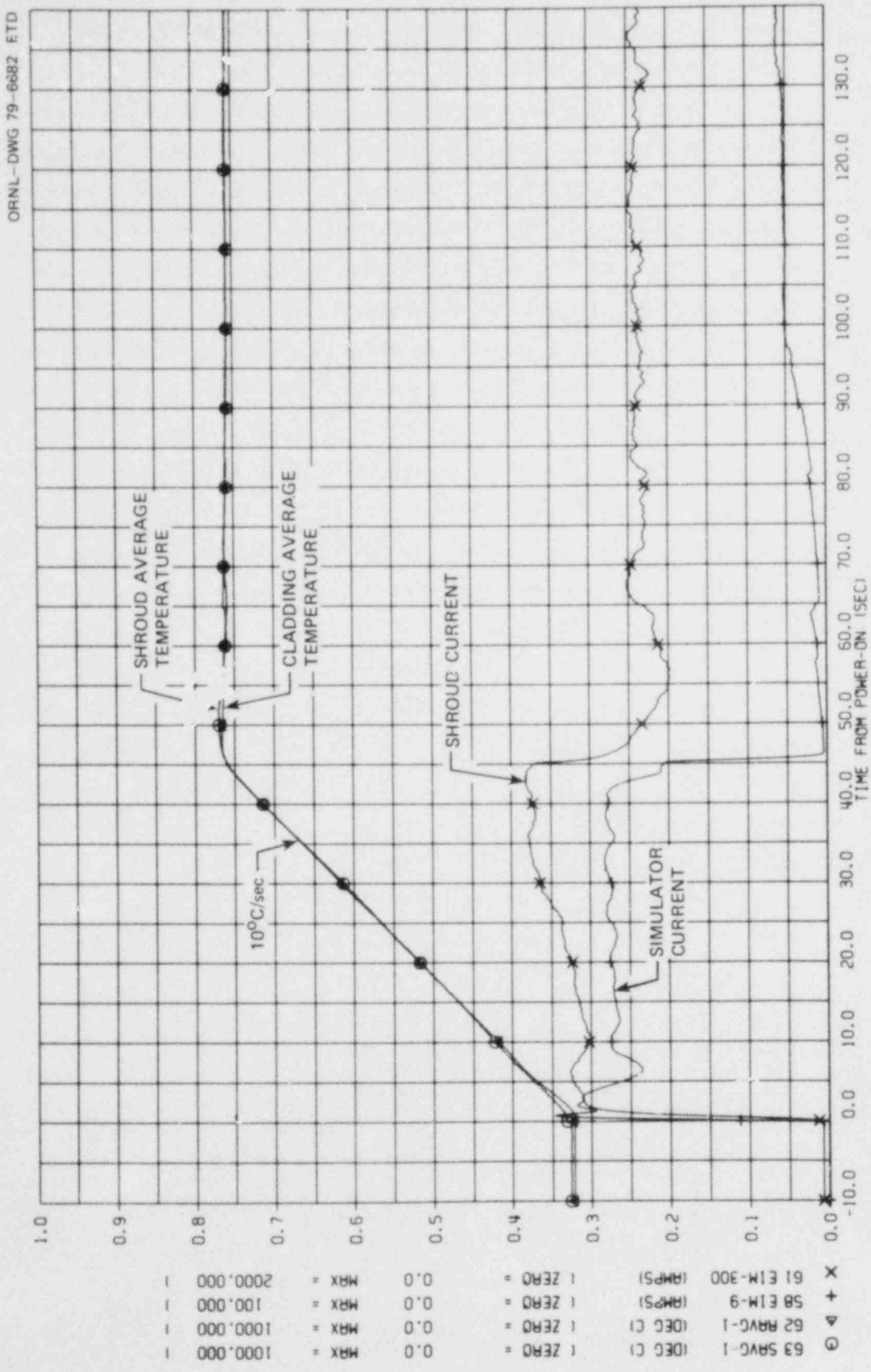

Fig. 3.5. Quick-look data plot of SR-30 D test showing measured shroud and fuel-pin simulator currents and average temperatures.

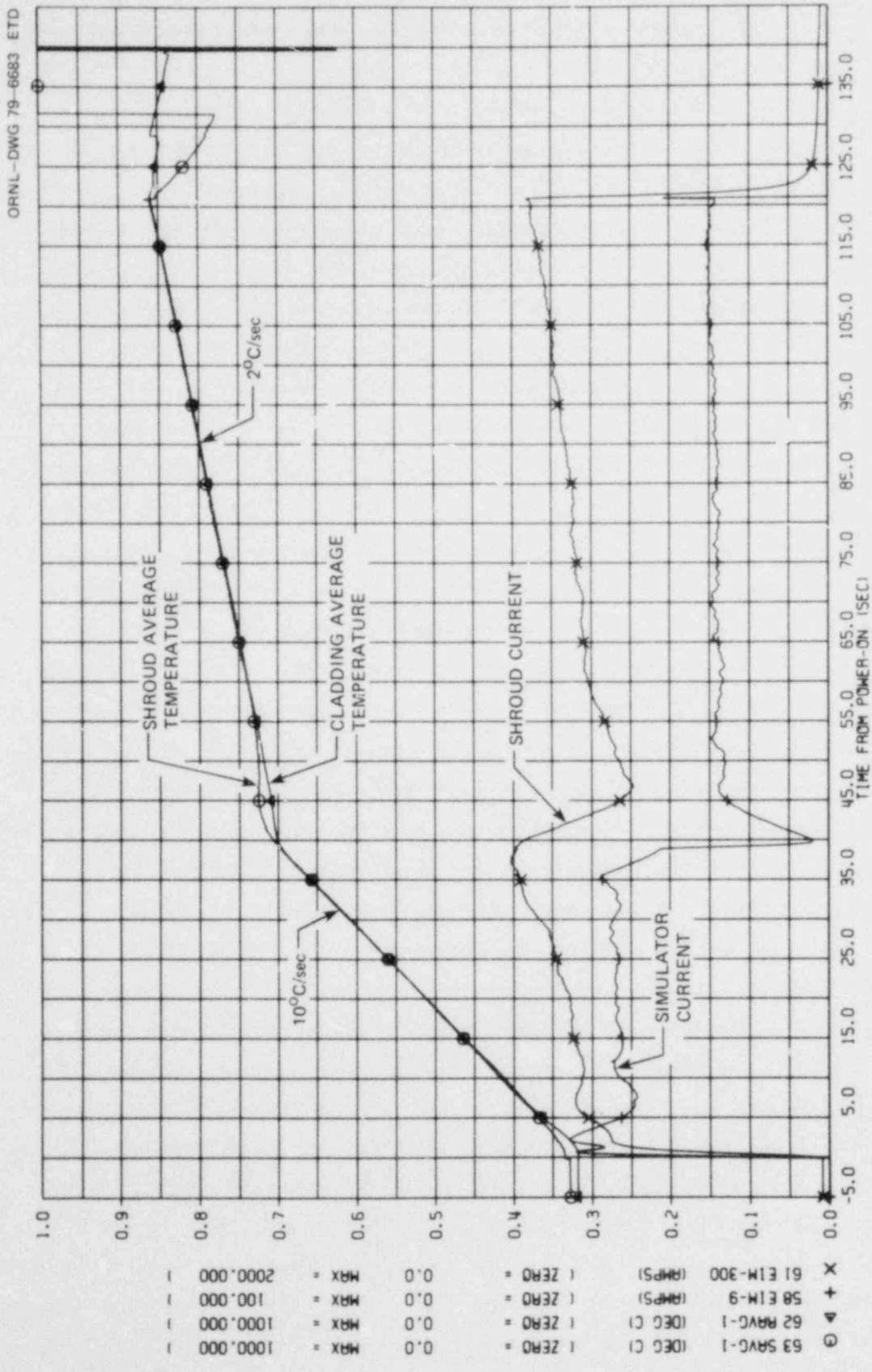

Fig. 3.6. Quick-look data plot of SR-30 I test showing measured shroud and fuel-pin simulator currents and average temperatures.

mid-May, has been delayed for a second time. Partial delivery of the order is expected in early August, with completion of the order by mid-September. Since this schedule created a severe impact on the schedule for assembling the fuel-pin simulators, we obtained about 330 m of bulk thermocouple material (from the same lot being used by the manufacturer to produce the 300 units on order) and initiated fabrication of thermocouples in house. The in-house fabrication procedure includes all the testing and acceptance inspection requirements, such as dye-penetrant inspection of the sheath, radiographic examination of the ungrounded sensing junction, and electrical resistance tests, included in the specification for the thermocouples on order.

The bulk material is sufficient to fabricate about 100 thermocouples, about one-third of the bundle requirements. The rate of in-house production and the number of thermocouples are such that fuel-pin simulator assembly will not be delayed.

We have experienced difficulties in the past with thermocouple signal offset associated with temperature measurements of the joule-heated shrouds in the bundle tests. Starting with the B4ST test assembly (and all future single-rod heated-shroud test assemblies), a new pretest checkout procedure was instituted to detect these problems before the test arrays are removed from the assembly area.

The procedure involves the use of a welding machine as a power source to provide 200 A dc for a short transient heating test on the shroud while the signal from each shroud thermocouple is recorded on a strip-chart recorder. In this test the thermocouple output signal is the sum of the thermoelectric voltage due to joule heating of the shroud by the current flowing through the shroud and the voltage gradient across the sensing junction due to the small bypass current flowing through the junction. The voltage gradient is detected by a step change in the recorded thermocouple output signal when the 200-A heating current is turned on or off. The signal is usually free of noise when the current is turned off, and this condition is used to determine the unbalanced voltage.

The sensing junction of the type S thermocouples is a more or less spherical ball with a diameter in the range of 500 to 750 μm. The voltage gradient along the 4 × 4 bundle shroud is typically about 20 μV/μm. Since

the thermoelectric output of the type S thermocouple is only about 10 μV/°C, it is readily apparent that significant temperature measurement errors will result unless the junction is attached so that the unbalanced voltage is essentially zero.

We have established acceptability limits on the unbalanced voltage (with the 200-A current flow) of the equivalent of a 2°C temperature measurement error on the bundle shroud thermocouples and of a 0.5°C error on shroud thermocouples in the single-rod test facility. If the unbalance voltage is greater than these limits, the junction is removed and re-welded. Normally, the unbalance voltage is brought within limits on the second attachment.

Data from the B4ST test series indicate that encasing the shroud thermocouple sheaths in heat-shrinkable Teflon tubing and other measures taken to increase the insulation resistance between the thermocouple wires and ground potential were successful in eliminating signal noise problems experienced in the B-1 and B-3 tests.

4. DESIGN, FABRICATION, AND EQUIPMENT MODIFICATIONS

4.1 Bundle B-5 Design

J. L. Crowley H. R. Payne*

The primary objectives of the test are to conduct a reasonably large bundle test under conditions that duplicate as nearly as possible those used in our single-rod and 4 × 4 bundle tests, so that the results can be considered representative of an infinite array and can serve as benchmarks for extrapolating and/or interpreting results from smaller test arrays.

These objectives are best satisfied by a test configuration that consists of an 8 × 8 array surrounded by a close-fitting, highly reflective, low-heat-capacity, unheated (i.e., without ohmic heating) shroud.

The close-fitting shroud will provide lateral restraint representing an adjacent row of rods that have deformed to the midpoint of the rod interval (about 32% deformation). Since the interval between tube surfaces is 3.5 mm, the shroud surface will be placed 1.75 mm from the outer row. This lateral restraint has not been present in earlier bundle tests. The very thin shroud will be supported by, but thermally insulated from, the support structure.

All the fuel-pin simulators will be identical in construction to those used in the previous bundle and single-rod tests. All the simulators will be pressurized to the same initial level, and all will be heated at the same rate (presently planned to be 10°C/sec). Each simulator will be instrumented with four internal thermocouples and a pressure transducer, the same as used in the previous bundle tests. In addition, each of four selected simulators in the B-5 assembly will be instrumented with four bare-wire (0.25-mm-diam) type S thermocouples equally spaced around the outside of the simulator and spot-welded to the Zircaloy tube to obtain circumferential temperature gradients.

---

*General Engineering Division.

A schematic drawing of the test configuration is given in Fig. 4.1. Detailed design of the bundle, which will be tested in the same vessel as was used for the earlier tests, is nearly complete.

4.2 B-5 Fuel-Pin Simulator Assembly

A. W. Longest

Assembly of fuel-pin simulators for the 8 × 8 bundle B-5 was started about midway of the current reporting period. The scheduled completion date is February 1, 1980. As in the case of the previous bundles, the Zircaloy tubes were selected, oxidized, and fitted with upper-end adapters beforehand. Fuel simulator (internal heater) preparation for B-5, which was started early in the previous report period, is continuing satisfactorily as described below. Fuel simulator preparation includes grooving to provide pathways for the FPS internal thermocouples, plasma spray coating of the heated zone with a protective coating of ZrO_2, and 10-sec infrared scanning to characterize axial heat generation distribution. For the 10-sec infrared scan, the fuel simulator (in a horizontal position in a holding fixture) is heated in air at a near-constant rate of about 38°C/sec from room temperature to about 400°C, at which time the infrared scan is performed while power is still on the fuel simulator.

The FPS design for B-5 is basically the same as for the previous 4 × 4 bundles. Four internal thermocouples are included in each FPS. The axial locations of these internal thermocouples were selected to provide an overall indication of the axial and radial temperature distributions in the test array. Sixteen FPS external thermocouples (0.25-mm bare-wire type S) are presently planned at one elevation in B-5 (four thermocouples, 90° apart, on each of four FPSs) to provide information concerning the azimuthal temperature differences during the test. FPS external thermocouples were not included in the B-1, B-2, and B-3 tests.

As described in the preceding progress report,[10] a group of 75 fuel simulators, all fabricated by the ORNL Fuel Rod Simulator Technology Laboratory,[6] were selected for preparation and possible use in B-5. The uniformity of the axial heat generation distributions of these simulators

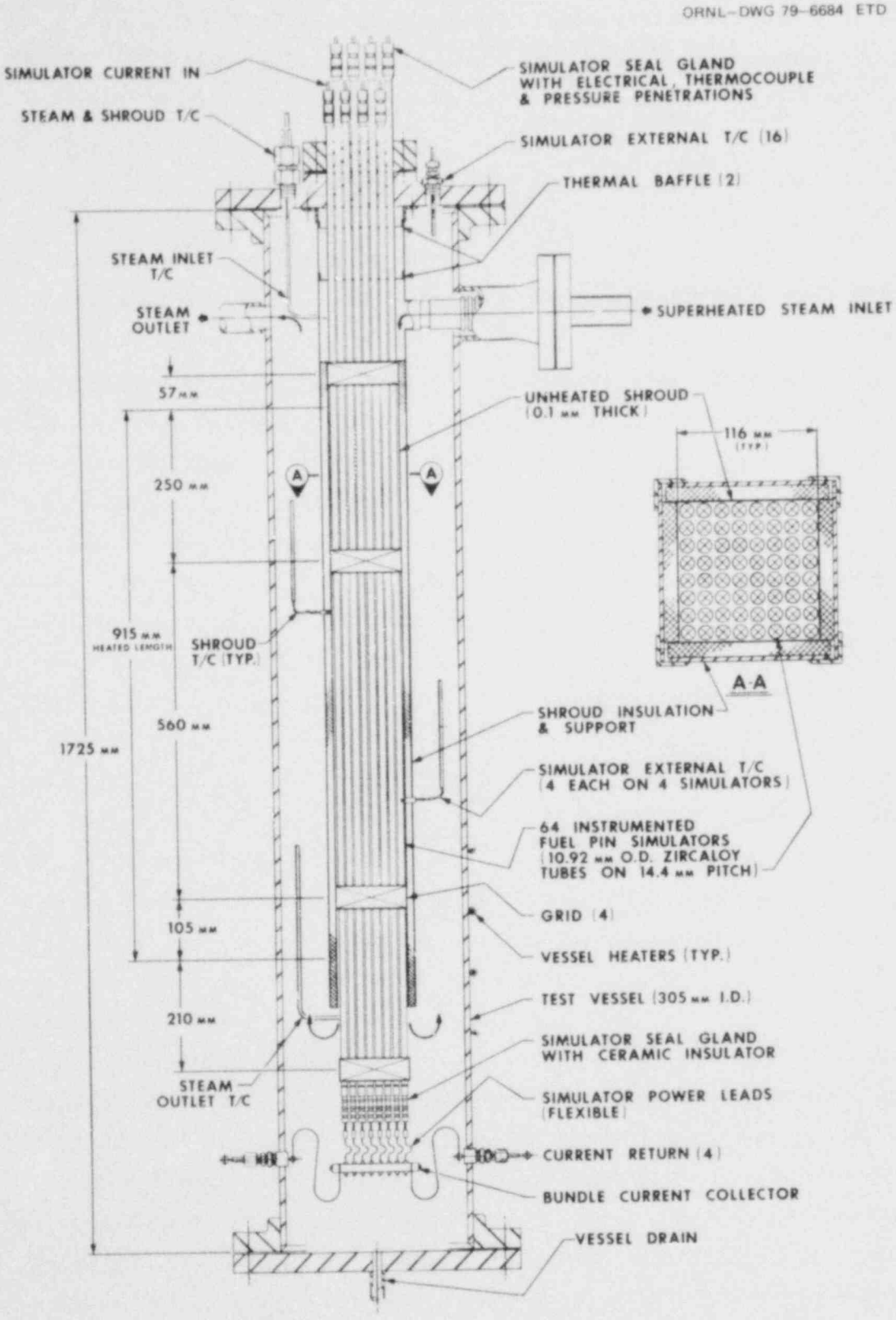

Fig. 4.1. Schematic of B-5 (8 x 8) bundle test assembly.

(as indicated by infrared scanning) is generally as good as or better than the best ones used in the previous 4 × 4 bundle tests.

An orderly progression of the fuel simulators through the three preparation stages of grooving, coating, and infrared scanning was in progress at the beginning of the current report period; 30 were grooved, 20 were ZrO_2 coated, and infrared scanning was scheduled to begin. At the end of this reporting period, 70 fuel simulators were grooved and approximately 50 of these were ZrO_2 coated and infrared scanned. Grooving inspection results showed that all the grooves were either within dimensional tolerances or sufficiently close to the specified tolerances to be acceptable for use in B-5. Likewise, coating inspection data indicated all coated simulators to be acceptable. However, a comparison of 10-sec infrared scans obtained before and after fuel simulator preparation showed that the ZrO_2 coatings introduced additional variations in the scans; a suspected cause is coating thickness variations. This was particularly noticeable on the B-5 group of fuel simulators because most of them showed 10-sec infrared scan variations before preparation of less than ±1.5% of the mean value. The more uniform the axial heat generation distribution, the more likely it is that imperfections or nonuniformity of the ZrO_2 coating will produce noticeable changes in the infrared scans. About one-third of the B-5 group of fuel simulators coated thus far have shown changes in the infrared scans that were greater than we judged to be acceptable based on results obtained immediately after checkout of the coating equipment. Those in this category were stripped of ZrO_2 and recoated (after checking and adjusting the coating equipment) with reasonably good results. The final postpreparation 10-sec infrared scan variations are generally less than ±2.5% of the mean value, compared with prepreparation variations of less than ±1.5% of the mean value.

As preparation of the fuel simulators is completed, they are assigned to the 64 positions in the bundle in much the same manner as was done for the previous bundle tests. In general, fuel simulators with the most uniform axial heat generation distributions, as indicated by the 10-sec infrared characterization scans, are assigned to the innermost positions and the least uniform ones to the outermost positions.

Essentially the same assembly techniques and procedures are being followed in assembling the B-5 simulators as were followed with the previous test assemblies. A completed copy of the assembly procedure, the drawings, and a full-length radiograph, provide the detailed as-built record for each individual simulator. These as-built data will be summarized and reported in a subsequent progress report when assembly of all the simulators has been completed.

4.3 Multirod Burst Test Facility Modifications

J. L. Crowley K. R. Carr*

Several modifications were made to the bundle test facility to (1) interface the control and signal cables to the new data acquisition system (DAS) and (2) provide the necessary connections and signal conditioning equipment for temperature-controlled experiments with the shroud heated by a separate power supply. Although the input signal connections to the new DAS are identical to those of the former DAS, the new DAS input connections are located about 20 m farther away from the test vessel. The required extra signal cable length was supplied by routing the existing signal cables to calibration cabinets installed and used by the Thermal Hydraulic Test Facility (THTF) and fabricating new cables to extend from the calibration cabinets on to the new DAS. There is now installed DAS input circuitry (multiplexers) for the exclusive use of the rod burst project. Formerly we shared the multiplexers of the host facility (THTF), and it was necessary to interchange the input connectors depending on which project was running an experiment.

Since the DAS is an integral part of the burst test control circuitry (the DAS is programmed to terminate an experiment when X thermocouples exceed a specified limit or Y rods have burst as indicated by the pressure decreasing below a specified limit), the new location of the DAS also required modification and relocation of associated control wiring.

Modifications made to accommodate temperature-controlled experiments with a separate shroud power supply included the installation of

---

*Instrumentation and Controls Division.

control and signal wiring between the various components of the temperature control system (bundle temperature controller and power supply, shroud temperature controller and power supply, temperature set-point generator, and existing control circuits). This wiring and the wiring and cooling water provision for the shroud power supply were designed for convenient removal of the controllers and power supply for subsequent use at the single-rod test facility.

In addition to the modifications described above, the facility expansion to test bundle B-5 (8 × 8) is now in progress. Equipment and components for which purchase requisitions have been submitted include thermocouple reference junction boxes, thermocouple extension wire and connectors, and pressure transducers. The facility expansion will provide a capability of about 300 thermocouple channels and 65 pressure channels. The total capability after the expansion will be 378 channels, which is expected to accommodate all future needs of the project. Electrical changes will be minor, involving increasing the size of return-current conductors and disconnecting cables previously used for shroud heating. (B-5 will not have an electrically heated shroud.) Additional helium manifolds, for pressurizing and monitoring the increased number of fuel-pin simulators in B-5, are presently being fabricated.

4.4 Data Acquisition and Software

K. R. Carr* F. R. Gibson*

The data acquistion and software activity during this quarter consisted mainly of operational support for completion of the B4ST test series and the initial single-rod heated-shroud experiments. In addition to operational support, we investigated an apparent electrical noise problem associated with the DAS channel that measured and recorded the shroud average temperature signal (identified as SAVG-1 on the plots) in the B4ST test series. This signal is characterized as high-level, 0–10 V dc corresponding linearly to 0–1000°C shroud average temperature.

---

*Instrumentation and Controls Division.

Some of the recorded data indicated noise spikes, typically negative, of several volts magnitude (see Fig. 3.3 for an example). The apparent noise occurred only during the period that heating power was applied to the experiment, which is also the period in which the DAS is in a particular mode of operation, and appeared to be associated with a characteristic range of SAVG-1 signal magnitudes. A strip-chart recorder connected in parallel with the DAS channel did not indicate noise on the SAVG-1 signal during the B4ST test series. Also, we have not experienced this problem in the single-rod tests, which utilize the same shroud temperature controller and power supply but a different DAS and simulator heater power supply.

Investigation of this problem included various hardware checks, such as interchanging the DAS input circuitry (multiplexer printed circuit boards) and simulating test conditions while monitoring the channel for noise with an oscilloscope. However, the noise did not appear with simulated test conditions. Later, THTF operations personnel experienced a problem with somewhat similar symptoms and found it to be caused by an internal operation of the DAS. With these new clues, we studied the software and data transfer operations of the DAS in the multirod test mode of operation but were unable to correlate the THTF problem and the multirod problem. We are continuing to investigate the source of apparent noise.

4.5 Single-Rod Test Facility Modifications

D. B. Lloyd

The single-rod test facility has been modified to include a heated-shroud capability. The essential elements of the new test assembly are shown in Fig. 4.2. As shown in the figure, the fuel-pin simulator is located in the center of the vessel and is surrounded by an Inconel 600 shroud. The simulator is freely suspended from the top flange to permit free downward expansion. The flange also includes penetrations for thermocouples, power leads, and steam lines as discussed below.

The shroud is connected electrically to an independently controlled dc power supply. Superheated steam is admitted to the annulus between

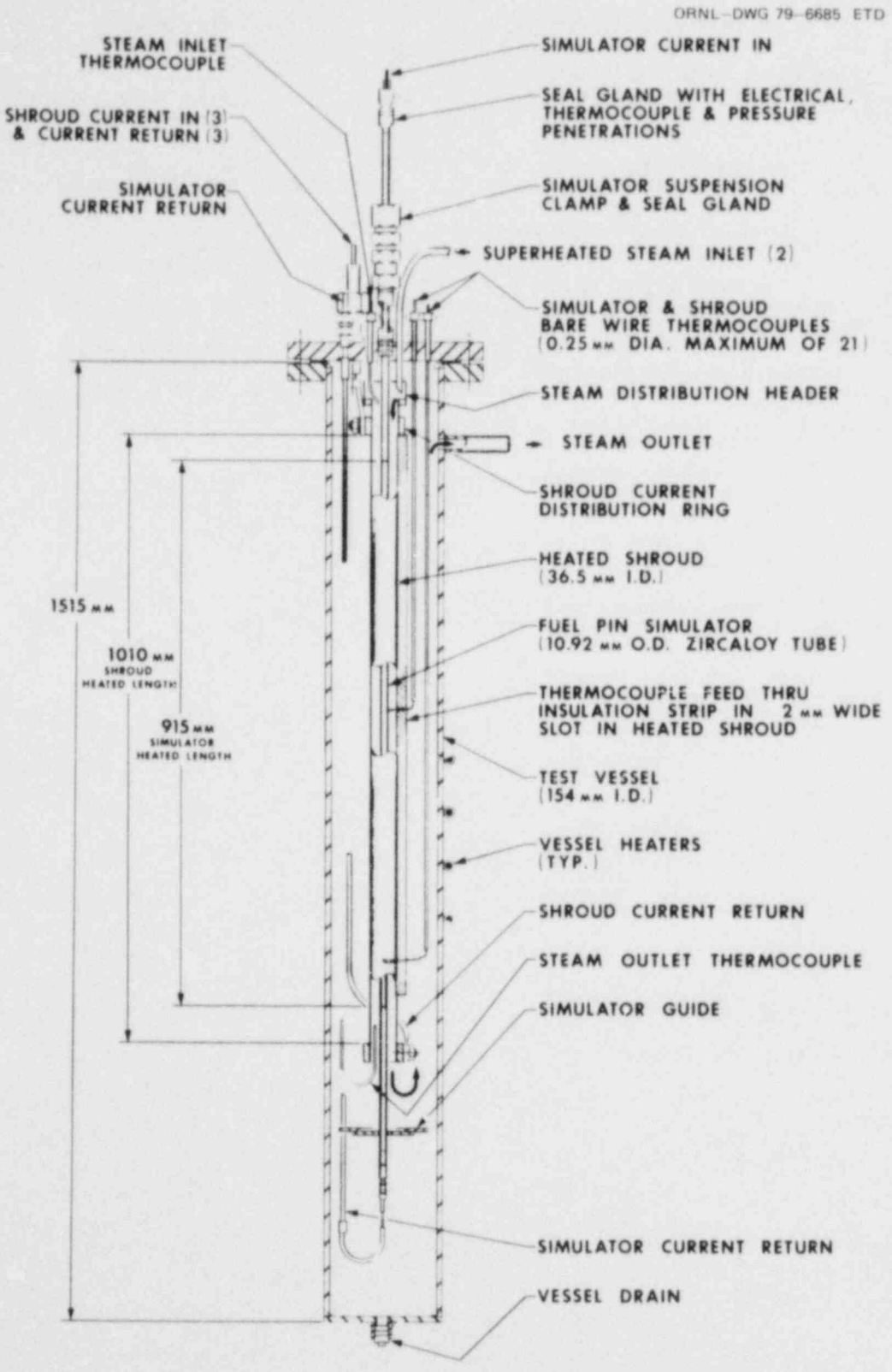

Fig. 4.2. Schematic of single-rod test assembly with heated shroud.

the fuel-pin simulator and the shroud through a steam distribution header at the top of the assembly. This header and the other shroud support members are designed so that the shroud is electrically isolated from the rest of the system. The steam flows downward through the annulus to the bottom of the shroud, back up along the outside of the shroud, and then through the steam outlet to a water-cooled condenser.

An insulation strip fitted into a narrow axial slot in the shroud provides access to the fuel-pin simulator for the thermocouples. The thermocouples exit the vessel through individual sealing glands mounted in the support flange.

A checkout assembly of the new components was made to assure proper fit-up and to familiarize project personnel with the new hardware. Several potential problems were identified and subsequently resolved during this operation. Figures 4.3–4.8 show details of different portions of the assembly.

Several calibration runs, covering the range of interest, were made to correlate the steam mass flow with the inlet pressure to the steam preheater. During these measurements a mockup assembly was installed in the vessel, the steam inlet and return lines were connected in the same manner as for a regular burst test, and the steam superheater and vessel were heated to normal pretest temperatures. The steam outlet of the vessel was connected to a water-cooled condenser, and the steam condensate was collected over measured time intervals to determine the steam mass flow rate.

The calibration data are plotted in Fig. 4.9 as Reynolds number in the flow annulus (between the fuel-pin simulator and the heated shroud) vs mass flow rate. The Reynolds number calculation assumed inlet steam at 340°C and 1 atm of pressure.

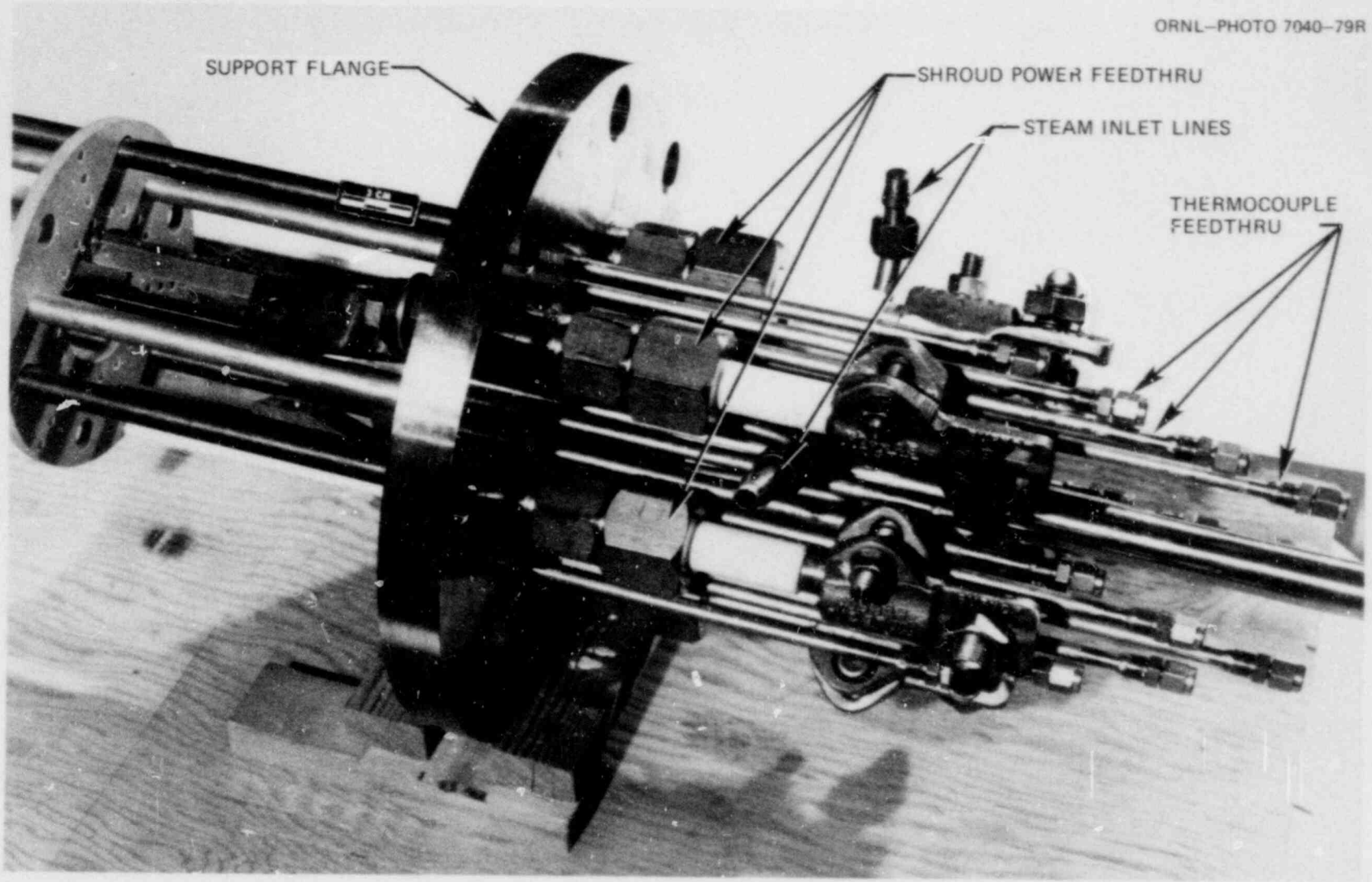

Fig. 4.3. Thermocouple, power, and steam connections on top of simulator support flange.

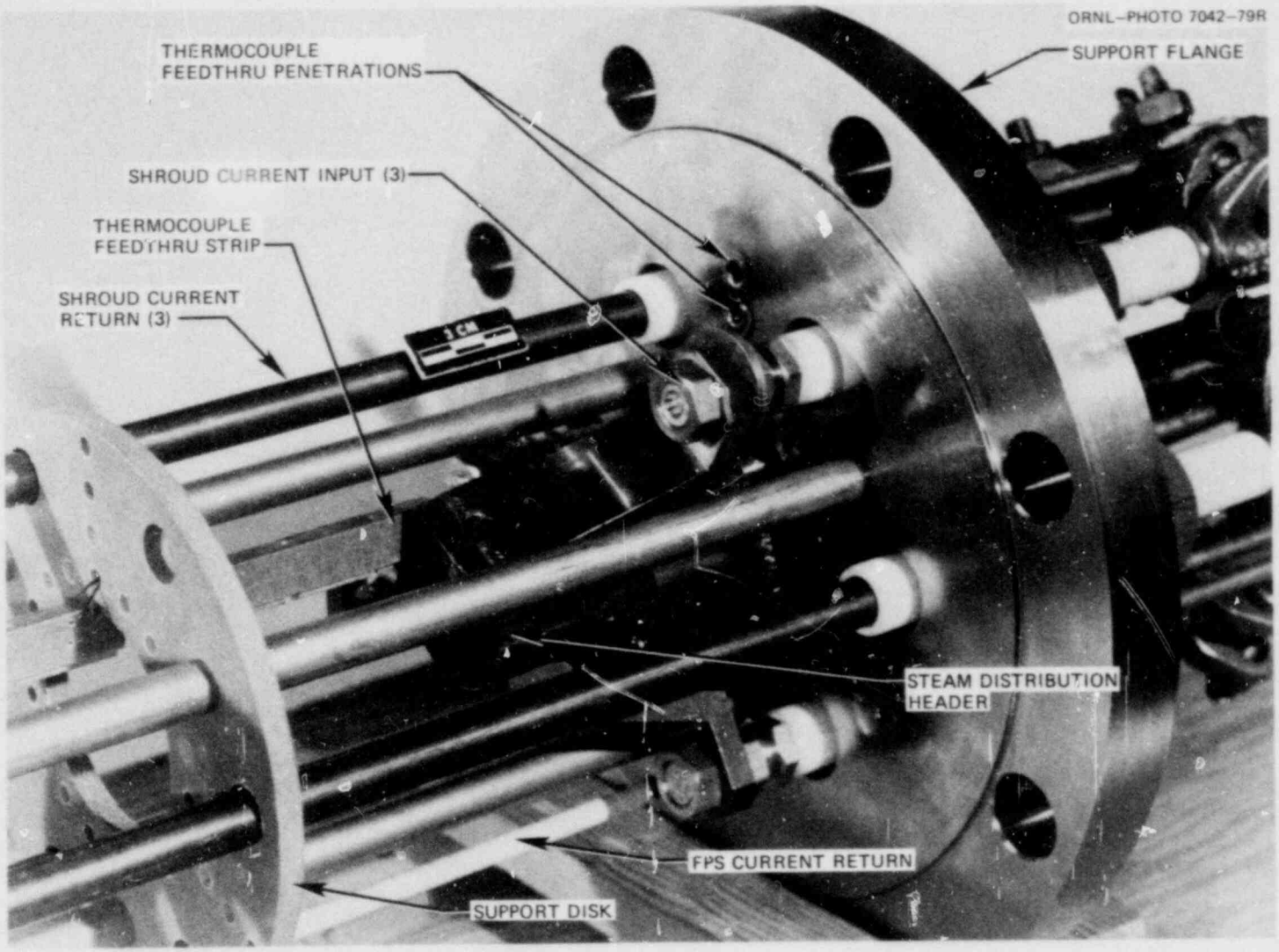

Fig. 4.4. Details of lower side of simulator support flange.

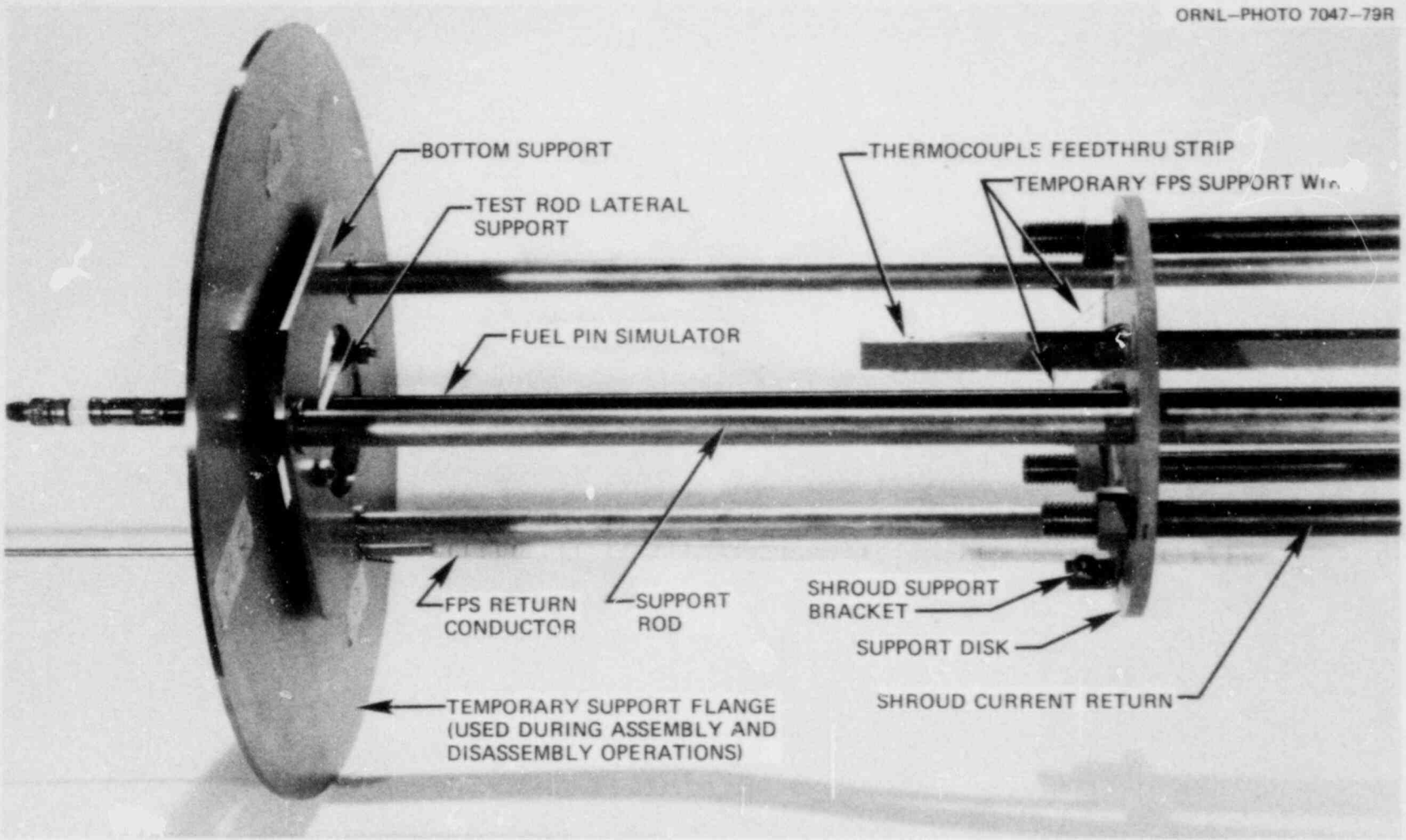

Fig. 4.5. Lower portion of simulator support system.

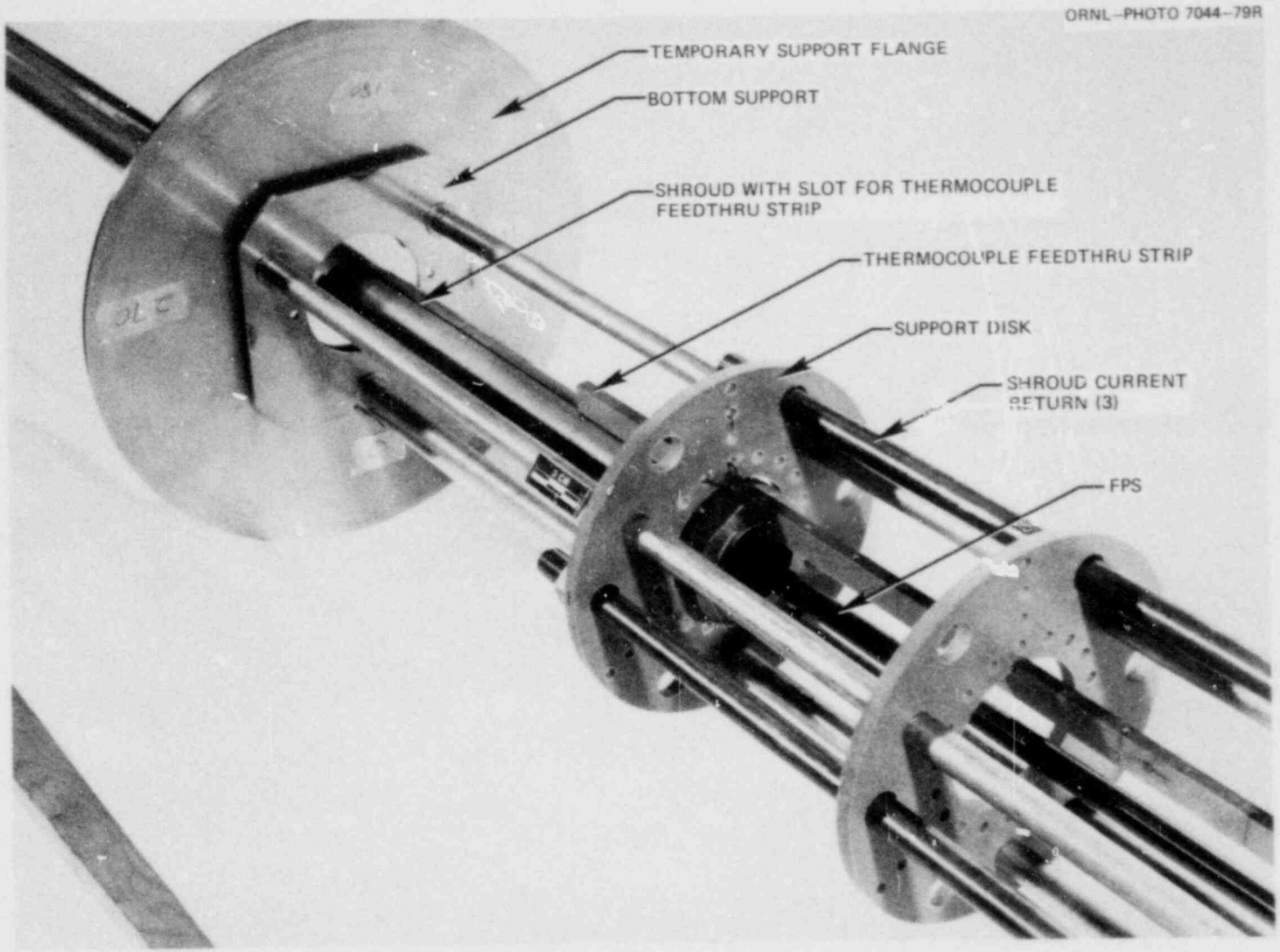

Fig. 4.6. Shroud being assembled over FPS and thermocouple feed-through strip.

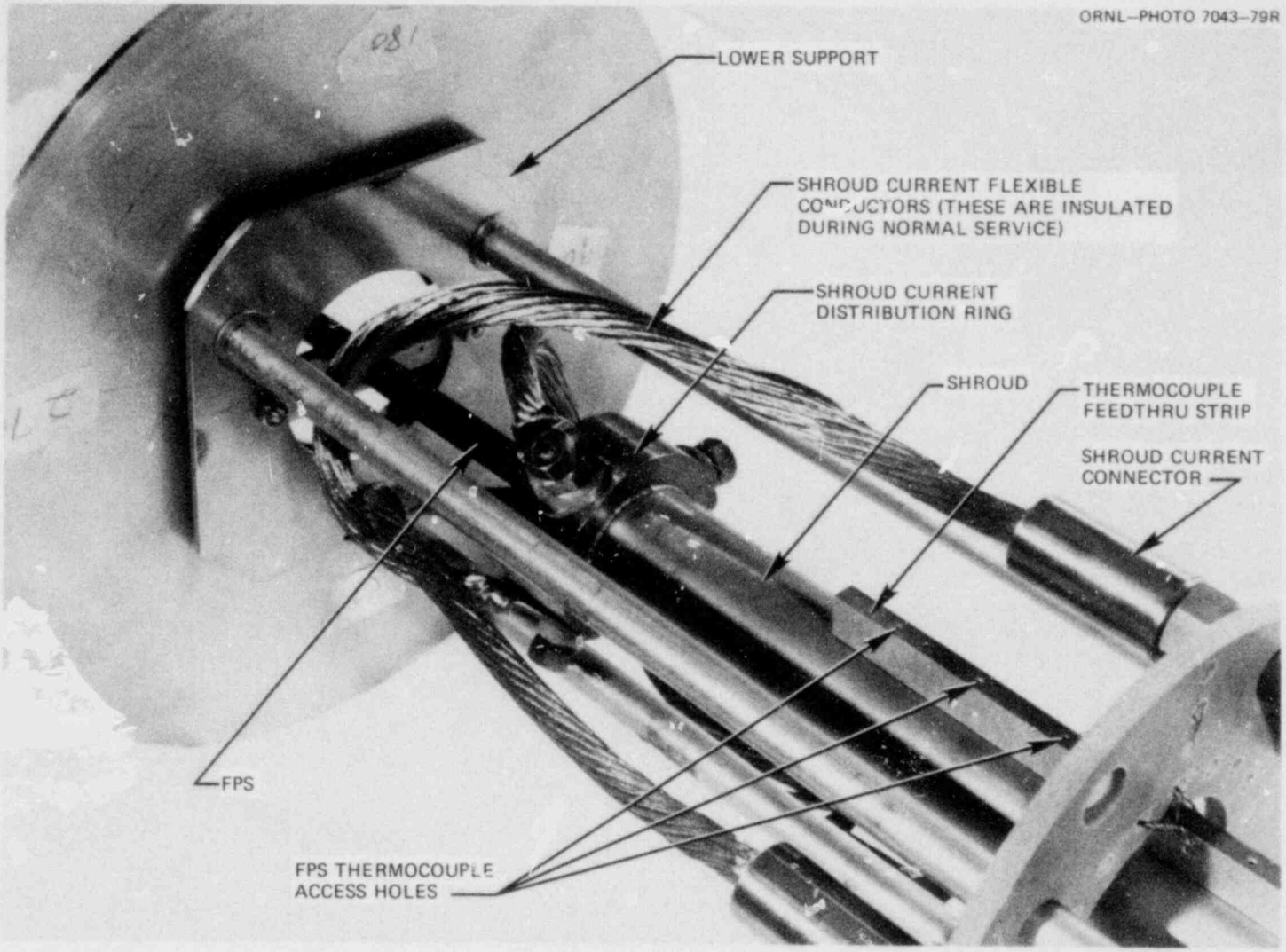

Fig. 4.7. Lower portion of assembly after installation of shroud.

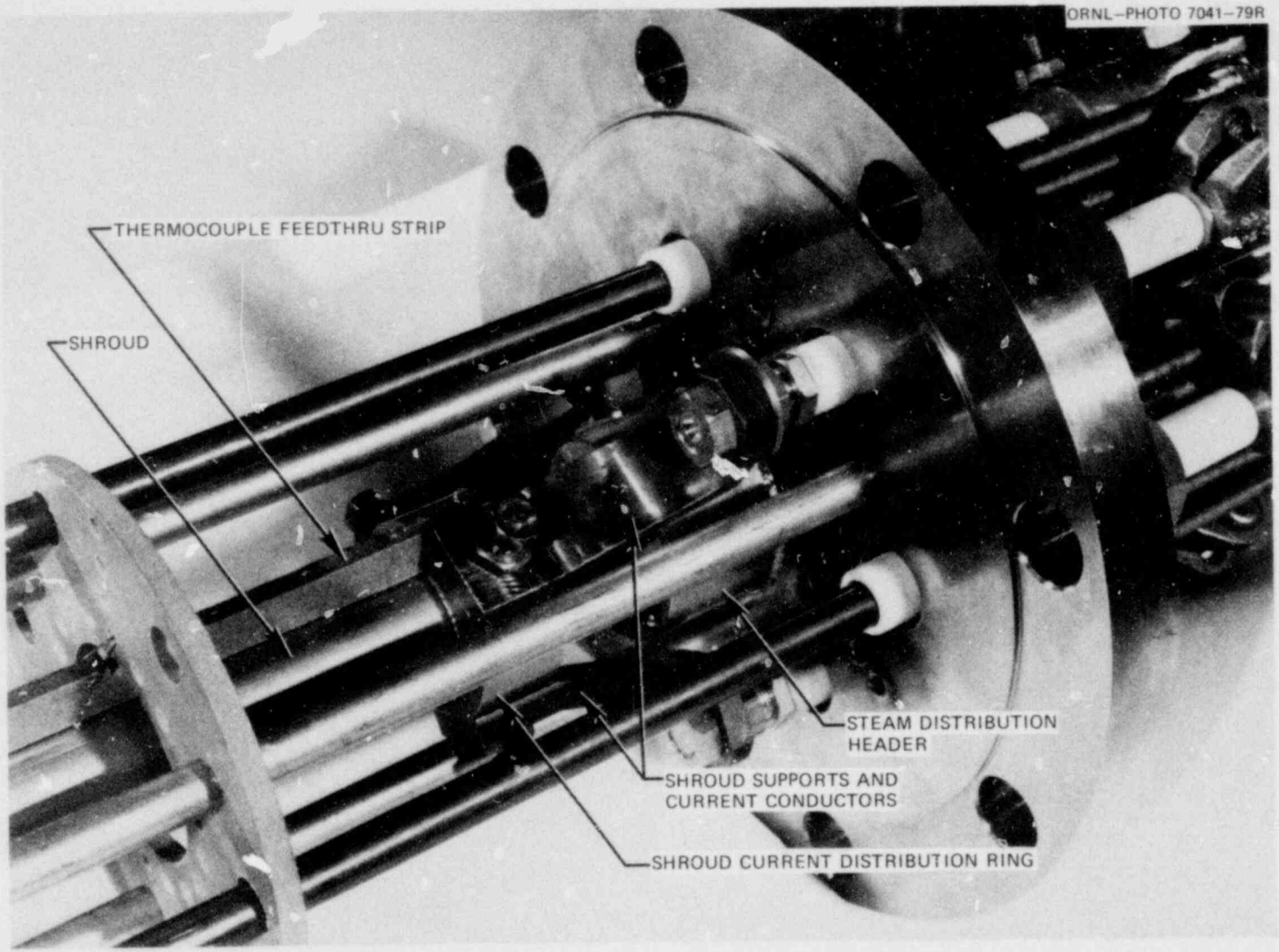

Fig. 4.8. Upper portion of assembly after installation of shroud.

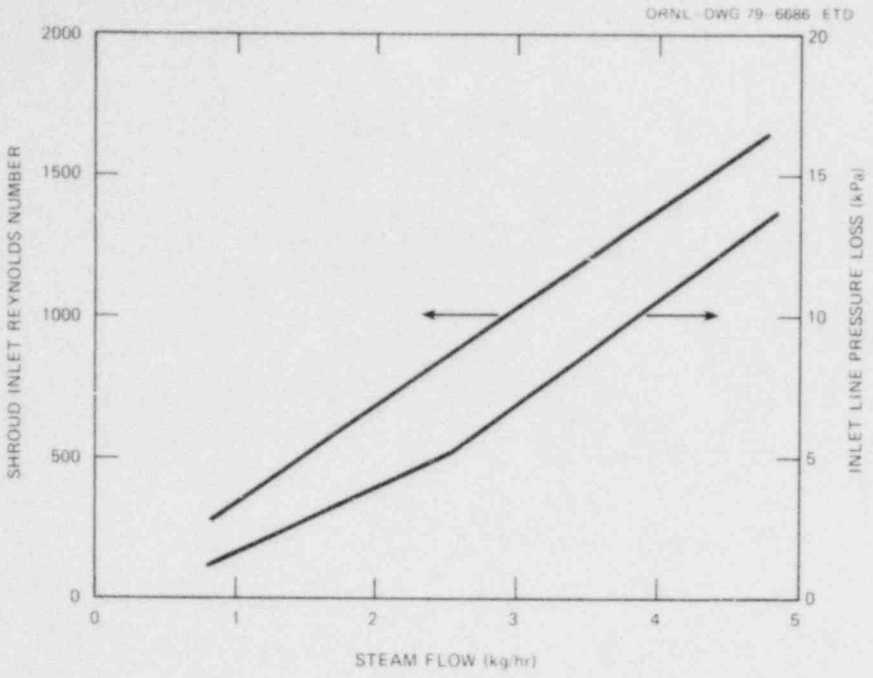

Fig. 4.9. Steam flow calibration results with the modified single-rod test assembly which is applicable to test No. SR-47 and subsequent tests. Shroud Reynolds number based on inlet conditions of 343°C and 1 atm of pressure.

5. OPERATIONS

J. L. Crowley K. R. Carr*
A. W. Longest

During this report period, shakedown and demonstration tests of the new shroud and fuel-pin simulator (FPS) temperature control systems were completed. These systems are designed to automatically control shroud and FPS temperatures along a preprogrammed path that may consist of a single linear temperature ramp to the tube burst temperature, a linear ramp to a specified temperature followed by a hold at that temperature, or a linear ramp followed by changeover to a second linear ramp having a different slope. Demonstration tests (see Sects. 3.2 and 3.3) have shown that the new control systems perform as designed and should provide adequate temperature control for both future bundle tests and heated-shroud single-rod tests.

Demonstration tests of the new temperature control systems in the multirod test facility were in progress at the end of the previous report period.[10] Those tests, using a sacrificial four-rod bundle designated B4ST, were successfully completed early in this report period and are discussed in Sect. 3.2.

Following the demonstration tests in the multirod test facility, the temperature control systems and the shroud portable power supply were moved to the single-rod test facility for similar tests in preparation for a planned series of heated-shroud single-rod tests. Facility modifications and fabrication of a new simulator test assembly which incorporates a heated shroud were completed on a schedule consistent with the equipment transfer and setup. A sacrificial FPS, designated SR-30, was installed into the new test assembly for use in these shakedown and demonstration tests. The SR-30 FPS was originally intended for use in bundle B-1 but had been set aside for single-rod use because of inoperative internal thermocouples. For monitoring the cladding temperatures in the demonstration tests, 12 external thermocouples were installed on FPS SR-30, with 4 equally spaced around the Zircaloy tube at each of three cross sections.

---

*Instrumentation and Controls Division.

The experience gained in setting up the power supplies and controllers in the B4ST tests in the multirod test facility helped considerably in setting up the new systems in the single-rod test facility. By the end of the report period, the planned series of SR-30 demonstration tests was completed. Sufficient information was obtained on controller system settings and operational procedures to permit initiation of a planned series of heated-shroud single-rod tests. The results of the SR-30 demonstration tests are presented and discussed in Sect. 3.3.

REFERENCES

1. R. H. Chapman, *Multirod Burst Test Program Quarterly Progress Report for January–March 1976*, ORNL/NUREG/TM-36.

2. R. H. Chapman, *Multirod Burst Test Program Quarterly Progress Report for April–June 1977*, ORNL/NUREG/TM-135.

3. R. H. Chapman, *Multirod Burst Test Program Progress Report for July–December 1977*, NUREG/CR-0103 (ORNL/NUREG/TM-200).

4. R. H. Chapman, *Multirod Burst Test Program Progress Report for January–March 1978*, NUREG/CR-0225 (ORNL/NUREG/TM-217).

5. R. H. Chapman et al., *Effect of Creep Time and Heating Rate on Deformation of Zircaloy-4 Tubes Tested in Steam with Internal Heaters*, NUREG/CR-0343 (ORNL/NUREG/TM-245) (October 1978).

6. R. H. Chapman, *Multirod Burst Test Program Progress Report for July–December 1978*, NUREG/CR-0655 (ORNL/NUREG/TM-297).

7. J. F. Mincey, *Steady-State Axial Pressure Losses along the Exterior of Deformed Multirod Burst Test (MRBT) Bundles B-1 and B-2*, ORNL/NUREG/TM-350 (in preparation).

8. R. H. Chapman et al., *Bundle B-1 Test Data*, ORNL/NUREG/TM-322 (June 1979).

9. R. H. Chapman et al., *Bundle B-2 Test Data*, ORNL/NUREG/TM-337 (August 1979).

10. A. W. Longest, *Multirod Burst Test Program Progress Report for January–March 1979*, NUREG/CR-0817 (ORNL/NUREG/TM-323).

11. R. H. Chapman et al., *Zirconium Cladding Deformation in a Steam Environment with Transient Heating*, in ASTM-STP-681 (1979).

12. D. G. Hardy, "High Temperature Expansion and Rupture Behavior of Zircaloy Tubing," in *Proceedings of ANS Topical Meeting on Water Reactor Safety, March 26–28, 1973, Salt Lake City, Utah*, CONF-730304.

13. S. Leistikow, *Halbjahresbericht 1976/2*, KfK-2345 (February 1977).

14. S. Leistikow, *Halbjahresbericht 1977/1*, KfK-2500 (December 1977).

15. P. Hofmann, *Influence of Iodine on the Strain and Rupture Behavior of Zry-4 Tubing at High Temperature*, in ASTM-STP-681 (1979).

16. K. M. Emmerich et al., *Failure of Pressurized Zircaloy Tubes during Thermal Excursions in Steam and in Inert Atmospheres*, in ASTM-STP-458 (1969).

NUREG/CR-1023
ORNL/NUREG/TM-351
Dist. Category R3

Internal Distribution

1. M. Bender
2. K. R. Carr
3-12. R. H. Chapman
13. W. G. Craddick
14. J. L. Crowley
15. H. L. Falkenberry
16. D. O. Hobson
17. Milton Levenson
18. D. B. Lloyd
19. A. W. Longest
20. A. P. Malinauskas
21. R. W. McCulloch
22. C. A. Mills
23. R. L. Moore
24. F. R. Mynatt
25. F. H. Neill
26. H. R. Payne
27-28. J. L. Rich
29. R. D. Stulting
30. H. E. Trammell
31. J. D. White
32. Patent Office
33. Nuclear Safety Information Center
34-35. Central Research Library
36. Document Reference Section
37-39. Laboratory Records Department
40. Laboratory Records (RC)

External Distribution

41. Office of Assistant Manager, Energy Research and Development, DOE, ORO
42. Director, Reactor Division, DOE, ORO
43. M. L. Picklesimer, Division of Reactor Safety Research, Office of Nuclear Regulatory Research, NRC, Washington, D.C. 20555
44. M. P. Bohn, EG&G Idaho, Inc., INEL, Idaho Falls, ID 83401
45. D. L. Hagrman, EG&G Idaho, Inc., INEL, Idaho Falls, ID 83401
46. R. R. Hobbins, EG&G Idaho, Inc., INEL, Idaho Falls, ID 83401
47. J. R. Larson, EG&G Idaho, Inc., INEL, Idaho Falls, ID 83401
48. C. R. Hann, BNWL, P.O. Box 999, Richland, WA 99352
49. M. Fischer, PNS-Leitung, Gesellschaft für Kernforschung, Postfach 3640, 75 Karlsruhe, FRG
50-51. Technical Information Center
52-391. Distribution as shown for NRC category R3 (NTIS-10)

* U. S. GOVERNMENT PRINTING OFFICE: 1979-640-245-284